nature immunology

RESOURCE

https://doi.org/10.1038/s41590-018-0291-z

Transcription factor Foxp1 regulates Foxp3 chromatin binding and coordinates regulatory T cell function

Catherine Konopacki[1,2,7], Yuri Pritykin[3,7], Yury Rubtsov[4,5], Christina S. Leslie[3*] and Alexander Y. Rudensky[1,2,6*]

Regulatory T cells (T_{reg} cells), whose differentiation and function are controlled by transcription factor Foxp3, express the closely related family member Foxp1. Here we explored Foxp1 function in T_{reg} cells. We found that a large number of Foxp3-bound genomic sites in T_{reg} cells were occupied by Foxp1 in both T_{reg} cells and conventional T cells (T_{conv} cells). In T_{reg} cells, Foxp1 markedly increased Foxp3 binding to these sites. Foxp1 deficiency in T_{reg} cells resulted in their impaired function and competitive fitness, associated with markedly reduced CD25 expression and interleukin-2 (IL-2) responsiveness, diminished CTLA-4 expression and increased SATB1 expression. The characteristic expression patterns of CD25, Foxp3 and CTLA-4 in T_{reg} cells were fully or partially rescued by strong IL-2 signaling. Our studies suggest that Foxp1 serves an essential non-redundant function in T_{reg} cells by enforcing Foxp3-mediated regulation of gene expression and enabling efficient IL-2 signaling in these cells.

Regulatory T cells (T_{reg} cells) play an essential role in limiting immune response-induced inflammation and associated pathology during infection and tissue injury[1]. The X-linked transcription factor Foxp3 is essential for establishment and maintenance of the T_{reg} cell lineage and suppressor function. Loss-of-function mutations in the *Foxp3* gene cause T_{reg} cell deficiency and consequent fatal multi-organ autoimmune and inflammatory disease in humans and mice[2–4].

Foxp3 is a member of the Foxp transcription factor subfamily (Foxp1–4), whose members regulate differentiation of a variety of cell types. All Foxp proteins contain a zinc finger domain and a leucine zipper motif amino (N)-terminal to the conserved DNA-binding forkhead domain[5]. The Foxp transcription factors are capable of homo- and heterodimerization, which is thought to enhance their binding to a relatively low-affinity consensus motif[6–8].

Besides the well-established role for Foxp3 in T_{reg} cell biology, another Foxp family member, Foxp1, plays an important role in the adaptive immune system by facilitating early B cell development, opposing follicular helper T cell (T_{FH} cell) differentiation, and maintaining quiescence of naïve T cells[9–12]. Foxp1 is highly expressed in naïve T cells and undergoes downregulation on their activation. Foxp1 forms homodimers and can also heterodimerize with Foxp3, which forms large protein complexes in T_{reg} cells that include Foxp1[13,14].

These observations prompted us to investigate whether Foxp3 might be binding predominantly to the sites occupied by Foxp1 in naïve T cells, replacing Foxp1 during T_{reg} cell differentiation. This scenario would imply that Foxp1 plays a redundant role in T_{reg} cells. Alternatively, it is possible that Foxp1 has a non-redundant function in T_{reg} cells through cooperative binding to sites occupied jointly with Foxp3 and involvement in Foxp3-mediated regulation of gene expression.

We found that Foxp1-bound sites in naïve $CD4^+$ T cells were largely overlapping with those found in T_{reg} cells, where the vast majority of Foxp1-bound sites were jointly occupied by Foxp3. T_{reg} cell-restricted Foxp1 deficiency resulted in a genome-wide reduction of Foxp3 binding and altered gene expression of a number of T_{reg} cell signature genes. Although T_{reg} cell-specific deficiency in Foxp1 did not result in severe autoimmune disease, it led to T_{reg} cell dysfunction, driven at least in part by sharply diminished CD25 expression and resultant impairment in IL-2 signaling. These results suggest that Foxp1 has a non-redundant role in T_{reg} cell fitness and suppressor function.

Results

Foxp1 and Foxp3 share a majority of binding sites. To determine whether Foxp3 and Foxp1 bound similar sites in T cells, we performed ChIP-seq in T_{reg} and naïve T_{conv} cells (Supplementary Tables 1 and 2). Foxp1 and Foxp3 ChIP-seq analyses identified 3,071 and 7,147 sites significantly bound by Foxp1 and Foxp3 in T_{reg} cells, respectively (FDR-adjusted $P < 0.01$, Fig. 1a). 1980 peaks were significantly bound by both Foxp1 and Foxp3, whereas 1,101 significantly bound Foxp3 peaks did not overlap with any Foxp1 peaks called at a relaxed threshold, and only 54 significantly bound Foxp1 peaks did not overlap with any Foxp3 peaks called at a relaxed threshold (Fig. 1a; see Methods). In naïve T_{conv} cells, we identified 1,088 significantly bound Foxp1 peaks (false discovery rate (FDR)-adjusted $P < 0.01$, Fig. 1b), over 95% of which were also bound by Foxp1 in T_{reg} cells at a relaxed threshold (Fig. 1b; see Methods). While more than half of Foxp3-bound sites were in intronic and intergenic regions, less than 30% of Foxp1-bound sites were in such regions. Rather, Foxp1 binding was primarily at promoters in T_{reg} cells (Fig. 1c). The remarkable overlap of Foxp3 and Foxp1 peaks is

[1]Howard Hughes Medical Institute, Memorial Sloan Kettering Cancer Center, New York, NY, USA. [2]Immunology Program, Memorial Sloan Kettering Cancer Center, New York, NY, USA. [3]Computational and Systems Biology Program, Memorial Sloan Kettering Cancer Center, New York, NY, USA. [4]Shemyakin–Ovchinnikov Institute of Bioorganic Chemistry, Russian Academy of Sciences, Moscow, Russia. [5]Faculty of Biology and Biotechnology, National Research University Higher School of Economics, Moscow, Russia. [6]Ludwig Center at Memorial Sloan Kettering Cancer Center, Memorial Sloan Kettering Cancer Center, New York, NY, USA. [7]These authors contributed equally: Catherine Konopacki, Yuri Pritykin. *e-mail: cleslie@cbio.mskcc.org; rudenska@mskcc.org

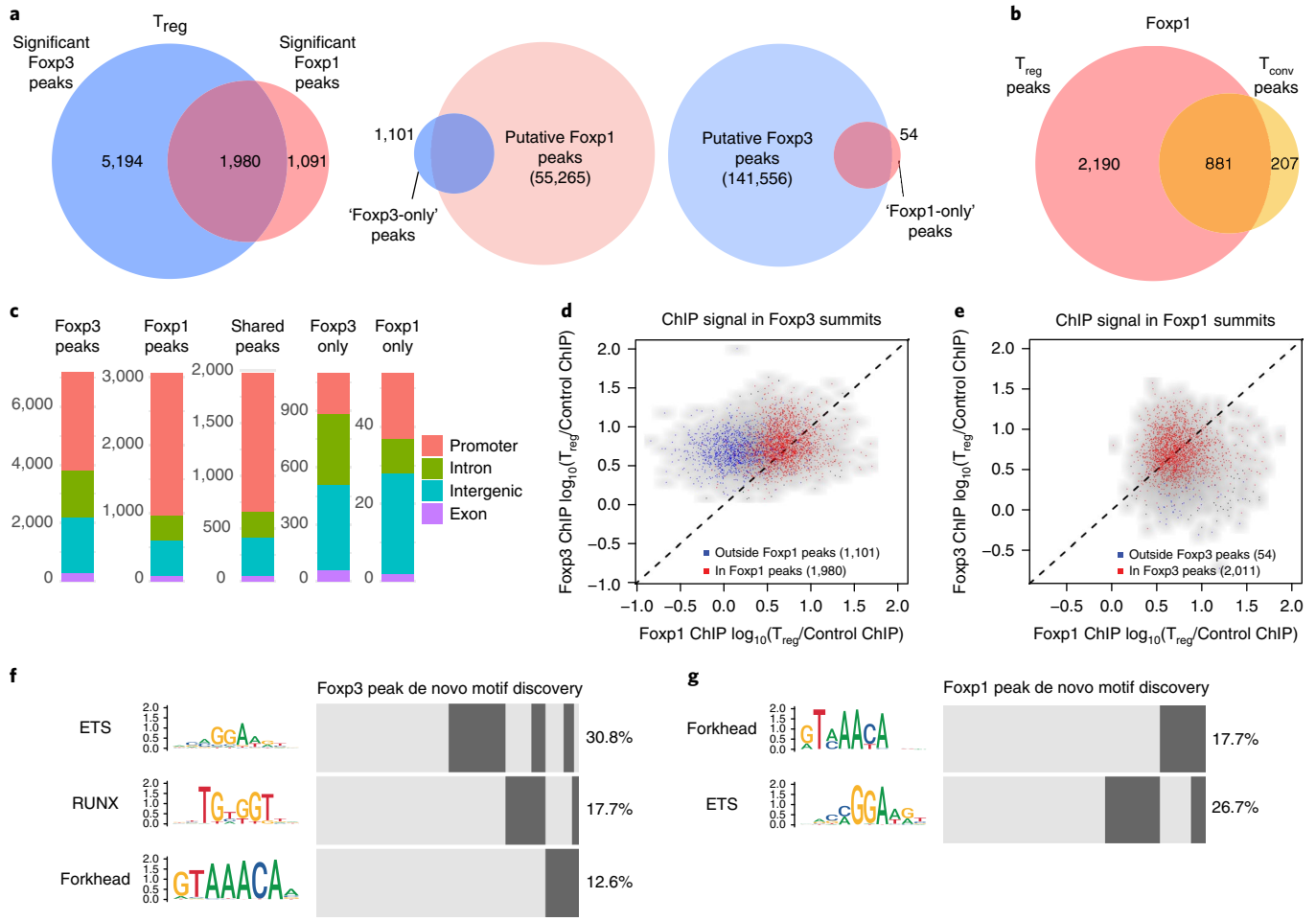

Fig. 1 | Foxp1 and Foxp3 share a majority of binding sites. a, Venn diagram of Foxp1- and Foxp3-bound sites in T_{reg} cells (FDR-adjusted $P < 0.01$) (left). Venn diagrams of significant Foxp1 and Foxp3 peaks not overlapping with putative peaks of the other transcription factor at a relaxed threshold ($P < 0.1$, see Methods) (middle and right). **b**, Venn diagram of Foxp1-bound sites in T_{reg} and T_{conv} cells (FDR-adjusted $P < 0.01$). **c**, Genomic distribution of Foxp1- and Foxp3-bound sites (FDR-adjusted $P < 0.01$). **d**, Scatter plot of Foxp3 and Foxp1 ChIP signal at Foxp3 summits. Data are shown for Foxp3 summits bound only by Foxp3 (blue) and Foxp3 summits that overlap with Foxp1 peaks (red). **e**, Scatter plot of Foxp3 and Foxp1 ChIP signal at Foxp1 summits. Data are shown for Foxp1 summits bound only by Foxp1 (blue) and Foxp1 summits that overlap with Foxp3 peaks (red). **f**,**g**, HOMER analysis of Foxp3- (**f**) and Foxp1- (**g**) bound sites to identify enriched transcription factor motifs. See Methods for detailed explanation of significant and putative peak calling.

noteworthy, as it is highly improbable for two unrelated ChIP-seq profiles to highly correlate with each other[15].

The ChIP signal for Foxp3 in T_{reg} cells at the summits of shared peaks was slightly stronger than the ChIP signal at peak summits bound only by Foxp3, while the opposite was true for Foxp1 (Fig. 1d,e and Supplementary Fig. 1). To identify motifs enriched within the Foxp3 and Foxp1 peaks, we performed de novo motif discovery using HOMER[16]. The canonical forkhead motif was most significantly enriched in Foxp1 ChIP-seq peaks, while in Foxp3 peaks Ets and Runx motifs were more significantly enriched than the forkhead motif, in line with our previous study[17] (Supplementary Fig. 1). Specifically, 12.6% of Foxp3 peaks and 17.7% of Foxp1 peaks contained the canonical forkhead motif (Fig. 1f,g). The forkhead motif occurred only once in the vast majority of peaks in which it was found. By accounting for all individual occurrences of the forkhead motif around peak summits using a relaxed motif hit threshold, we found 1,625 Foxp3 peaks out of 7,174 with at least one forkhead motif occurrence. However, only 102 Foxp3 peaks (1.4% of all) contained two or more occurrences of the forkhead motif, which is not more than expected by chance if the forkhead motifs were randomly placed among peaks (see Methods). Of these 102 peaks, 57 peaks contained the two forkhead motifs at a distance 20 base pairs (bp) or larger. Thus, it is unlikely that both forkhead domains of Foxp3 homodimers bind simultaneously to DNA at two closely adjacent forkhead motifs[18], although they may mediate long-range chromatin interactions by bridging two separate DNA sites, which would require only one forkhead motif per regulatory element[19]. Finally, it is also possible that one dimer member mediates the interaction with DNA at a given time. Foxp1 and Foxp3 peaks contained Ets family motifs (26.7% and 30.8%, respectively) and 17.7% of Foxp3 peaks contained Runx motifs (Fig. 1f,g). The observation of a relatively small percentage of Foxp1 and Foxp3 peaks with a forkhead motif supports previous reports that other transcription factor(s) present in the Foxp3 protein complexes may contribute to DNA binding[20,21]. Thus, Foxp1 binds predominantly to the sites bound by Foxp3.

Foxp3 DNA binding is reduced in the absence of Foxp1. We considered that loss of Foxp1, and the resulting inability of Foxp3 to form heterodimeric protein complexes with Foxp1, could lead to a reduction in Foxp3 binding specifically at sites occupied by both Foxp3 and Foxp1. Alternatively, the reduced abundance of total Foxp ('1+3') protein due to loss of Foxp1 could lead to reduced

Foxp3 binding at all genomic sites due to redistribution of Foxp3 protein. To distinguish between these two possibilities, we generated a novel conditional *Foxp1* allele and combined it with the previously described *Foxp3*$^{YFP\text{-}Cre}$ allele to obtain mice with T_{reg} cell-restricted Foxp1 deficiency (Supplementary Fig. 2). Foxp3 ChIP-seq analysis of Foxp1-deficient and -sufficient T_{reg} cells using background noise normalization in all replicates for multiple sample comparison of ChIP signal (see Methods) revealed that the number of sites significantly bound by Foxp3 was reduced in T_{reg} cells lacking Foxp1 (Fig. 2a). Furthermore, Foxp3 ChIP signal was predominantly reduced in Foxp1-deficient T_{reg} cells at all Foxp3-bound sites and not only at sites bound by Foxp1 (Fig. 2b). This result suggested that Foxp1 deletion in Foxp3-expressing cells may lead to a redistribution of Foxp3 genome wide (Fig. 2c). Foxp1 expression in T cells is induced at the double negative 2 stage, and we observed that Foxp1 expression was high in T_{reg} precursor cells (Fig. 2d).

To exclude the possibility that decreased Foxp3 genome occupancy might be due to a change in Foxp3 protein abundance, we assessed Foxp3 protein content in Foxp1-deficient and -sufficient resting CD62L^{hi} T_{reg} cells and activated CD44^{hi} T_{reg} cells using flow cytometry. We observed a modest reduction in Foxp3 protein abundance in Foxp1-deficient naïve T_{reg} cells and unaltered Foxp3 protein amounts in Foxp1-deficient activated T_{reg} cells, compared with their Foxp1-sufficient counterparts (Fig. 2e,f). Foxp3 messenger RNA abundance was also reduced in Foxp1-deficient T_{reg} cells, suggesting that the decrease of Foxp3 protein in Foxp1-deficient cells may be due to altered transcriptional regulation of Foxp3 (Supplementary Table 3). Foxp3 protein abundance and genome occupancy in highly activated T_{reg} cells was increased in comparison with resting T_{reg} cells (12,961 versus 7,497 Foxp3 peaks[22]; J. van der Veeken, Y.P. and A.Y.R, unpublished observations) while Foxp1 protein abundance was decreased. It is noteworthy that a larger percentage of Foxp1-deficient T_{reg} cells exhibited an activated phenotype compared with Foxp1-sufficient T_{reg} cells, and thus the majority of Foxp1-deficient T_{reg} cells expressed more Foxp3 protein on a per cell basis than Foxp1-sufficient T_{reg} cells. However, in contrast to Foxp1-sufficient activated T_{reg} cells, Foxp1-deficient T_{reg} cells exhibited fewer significant Foxp3 peaks than Foxp1-sufficient counterparts (3,935 versus 7,174 peaks). These observations are consistent with our proposed 'dilution' model for diminished Foxp3 binding in the absence of Foxp1.

Foxp1-dependent regulation of gene expression in T_{reg} cells. To assess the impact of Foxp1 loss on T_{reg} gene expression, we performed RNA-seq of YFP$^+$ CD62L^{hi} naïve or CD44^{hi} activated T_{reg} cells (Supplementary Table 3). Since we observed that *Foxp3*$^{YFP\text{-}Cre}$ *Foxp1*$^{fl/fl}$ mice exhibited moderate immune activation, we performed RNA-seq analysis of T_{reg} cells isolated from healthy heterozygous *Foxp3*$^{YFP\text{-}Cre/+}$ *Foxp1*$^{fl/fl}$ or *Foxp3*$^{YFP\text{-}Cre/+}$ *Foxp1*$^{+/+}$ female mice harboring both Foxp1-deficient and -sufficient T_{reg} cells as the result of random X-chromosome inactivation. We performed *k*-means clustering of genes that were bound by Foxp1 in T_{reg} cells and that were differentially expressed between Foxp1-deficient and Foxp1-sufficient T_{reg} cells (FDR-adjusted $P < 0.01$) and performed gene ontology pathway analysis for the six clusters identified (Fig. 2g, Supplementary Fig. 3 and Supplementary Table 4). Cluster 3 included genes that were downregulated in the absence of Foxp1 in both naïve and activated T_{reg} cells, including T_{reg} signature genes *Il2ra* and *Ikzf4*. Cluster 1 was enriched for genes associated with skeletal and heart muscle, reproductive organ development and adrenal cortex formation. Foxp1 is known to play an essential role in these developmental processes[23–26]. Accordingly, we found a number of genes linked to development of these organs, including *Arntl*, *Cited2*, *Hdac4*, *Nr4a1*, *Chd7*, *Dnajb6*, *H3f3b* and *Spo11*, differentially expressed in Foxp1-deficient T_{reg} cells and directly bound by Foxp1. Foxp1 binding to these gene loci have not been previously described, with the exception of *Cited2*[27]. These findings suggest that Foxp1 may directly regulate expression of these genes and thereby affect both embryonic development and T_{reg} cell function. Cluster 5 included genes that were more highly expressed in activated T_{reg} cells and were downregulated in Foxp1-deficient T_{reg} cells compared with Foxp1-sufficient T_{reg} cells. This cluster included T cell activation genes *Cd83, Ctla4, Ikzf3, Hivep3, Nfatc1, Nfkb2, Prdm1, Relb, Rora* and *Smad3*, and was enriched for immune system development, leukocyte activation, regulation of gene expression and positive regulation of apoptotic signaling pathways.

Genes that were differentially expressed between Foxp1-sufficient and -deficient naïve and activated T_{reg} cells and that were bound by Foxp3 more prominently in Foxp1-sufficient T_{reg} cells included *Itga6*, *Smad7* and *Satb1* (Fig. 3a and Supplementary Tables 2 and 3). Most of these genes were also bound by Foxp1. Using a previously published T_{reg} gene signature that identified 407 overexpressed and 196 underexpressed genes, we found 136 genes overexpressed ('T_{reg} up') and 51 genes underexpressed ('T_{reg} down') that were associated with Foxp1 or Foxp3 ChIP-seq peaks (Fig. 3b,c and Supplementary Table 5)[28]. The 'T_{reg} up' genes were significantly more highly expressed in Foxp1-sufficient T_{reg} cells, while the 'T_{reg} down' genes were more highly expressed in Foxp1-deficient T_{reg} cells (Fig. 3b). In T_{reg} cells, expression of the genome organizer SATB1 is repressed in a Foxp3-dependent manner and this repression is important for their function[29]. Ectopic expression of SATB1 led to a loss of suppressive function and production of effector T cell cytokines[30]. Foxp1-deficient T_{reg} cells expressed more SATB1 at the mRNA and protein level than wild-type T_{reg} cells (Fig. 3c-e). To determine whether Foxp1 regulates *Satb1* expression in T_{conv} cells, we measured SATB1 expression in Foxp1-deficient T_{conv} cells from *Cd4*^{Cre} *Foxp1*$^{fl/fl}$ mice using flow cytometric analysis and found it to be unchanged (Supplementary Fig. 5). We found that Foxp1 and Foxp3 were both bound to two alternative forkhead motifs containing *Satb1* promoters in T_{reg} cells, and Foxp3 binding at these promoters was markedly diminished in Foxp1-deficient T_{reg} cells (Fig. 3f). Together these data suggest that, in addition to Foxp3, Foxp1 plays a specific non-redundant role in repression of *Satb1* in T_{reg} cells.

Foxp1-deficient T_{reg} cells produce effector cytokines. T_{reg} cell-restricted Foxp1 deficiency resulted in mild lymphadenopathy (Fig. 4a), which was in contrast to the reduced cellularity of spleens and lymph nodes of *Cd4*^{Cre}*Foxp1*$^{fl/fl}$ T cells (Supplementary Fig. 4)[11]. The proportion of CD4$^+$ T cells that were Foxp3$^+$ in lymph nodes was reduced approximately twofold (Fig. 4b,c). Foxp1-deficient T_{reg} cells were strongly activated on the basis of CD44 expression and exhibited higher proliferative activity than their Foxp1-sufficient counterparts, as measured by Ki-67 expression (Fig. 4d,e). Foxp1-deficient T_{reg} cells also produced more interferon-γ (IFN-γ) on phorbol 12-myristate 13-acetate (PMA) and ionomycin stimulation in vitro in comparison with control T_{reg} cells (Fig. 4f). These characteristics of activation were similar to those observed in Foxp1-deficient CD4$^+$ and CD8$^+$ T cells (Supplementary Fig. 4)[11].

Activation of Foxp1-deficient CD4$^+$ and CD8$^+$ T cells was linked to elevated expression of IL-7 receptor (IL7R) due to derepression of the *Il7ra* locus and heightened IL-7-dependent proliferation[11]. Foxp3 is also known to regulate expression of IL7R α-chain (IL-7Rα). Thus, we investigated whether Foxp1 deficiency in T_{reg} cells resulted in increased cell surface IL7R expression and proliferation in response to IL-7. We found that neither was affected by Foxp1 deficiency in T_{reg} cells, probably because Foxp3 binding to the *Il7ra* locus was not reduced in the absence of Foxp1 (Supplementary Fig. 5). Thus, while Foxp1 deficiency results in activation of T_{conv} and T_{reg} cells, the mechanisms underlying their activation appear to be distinct.

Foxp1 deficiency causes T_{reg} cell functional impairment. The gene expression analysis of Foxp1-deficient T_{reg} cells revealed

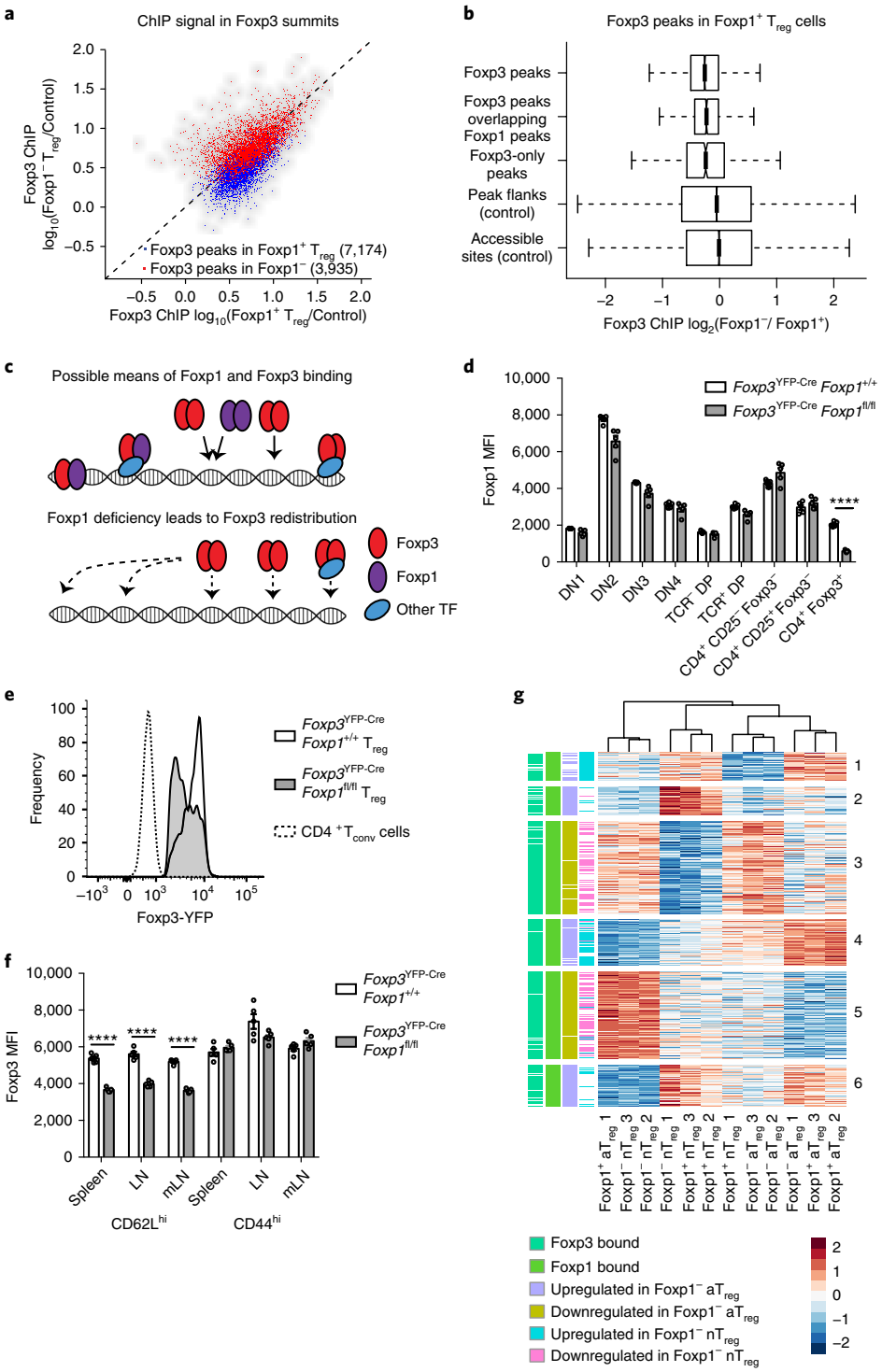

Fig. 2 | Foxp3 DNA binding is reduced in the absence of Foxp1. a, Scatter plot of Foxp3-bound sites in Foxp1$^+$ and Foxp1$^-$ T_{reg} cells (FDR-adjusted $P < 0.01$). See Methods for detailed explanation of significant peak calling. **b**, Box plot of Foxp3 ChIP binding intensity in Foxp1$^-$/Foxp1$^+$ T_{reg} cells at peaks that overlap with Foxp1 peaks ($n = 1{,}980$), at Foxp3-only peaks ($n = 1101$), at all Foxp3 peaks ($n = 7{,}174$), at peak flanks ($n = 241{,}691$), and at all accessible sites ($n = 101{,}224$). Box shows interquartile range (IQR) of a sample centered at median, notches show a confidence interval around the median estimated as median $\pm 1.57 \times \text{IQR}/(\sqrt{\text{sample size}})$, whiskers extend IQR endpoints by $1.5 \times$ IQR in each direction, outliers beyond interval between whiskers are omitted from the plot. **c**, Schematic representation of Foxp3 redistribution in absence of Foxp1. **d**, Summary plot of Foxp1 mean fluorescence intensity (MFI) in thymic cell subsets from 8- to 10-week-old male mice ($n = 5$ biologically independent mice per group, representative of three independent experiments, error bars represent s.e.m. centered on the mean, $^{****}P < 0.0001$, unpaired two-tailed Student's t-test). **e**, Representative histogram of Foxp3 protein level in naïve Foxp1$^+$ and Foxp1$^-$ T_{reg} cells and in naïve T_{conv} cells from pooled skin-draining lymph nodes (representative of three independent experiments). **f**, Summary plot of Foxp3 MFI in Foxp1$^+$ and Foxp1$^-$ T_{reg} cells from 8- to 10-week-old male mice ($n = 5$ biologically independent mice per group, representative of three independent experiments, error bars represent s.e.m. centered on the mean, $^{****}P < 0.0001$, unpaired two-tailed Student's t-test). **g**, Heat map of differentially expressed (FDR-adjusted $P < 0.01$) genes associated with Foxp1 peaks clustered using k-means clustering. Statistical significance test of differentially expressed genes is described in detail in Methods and is two-sided.

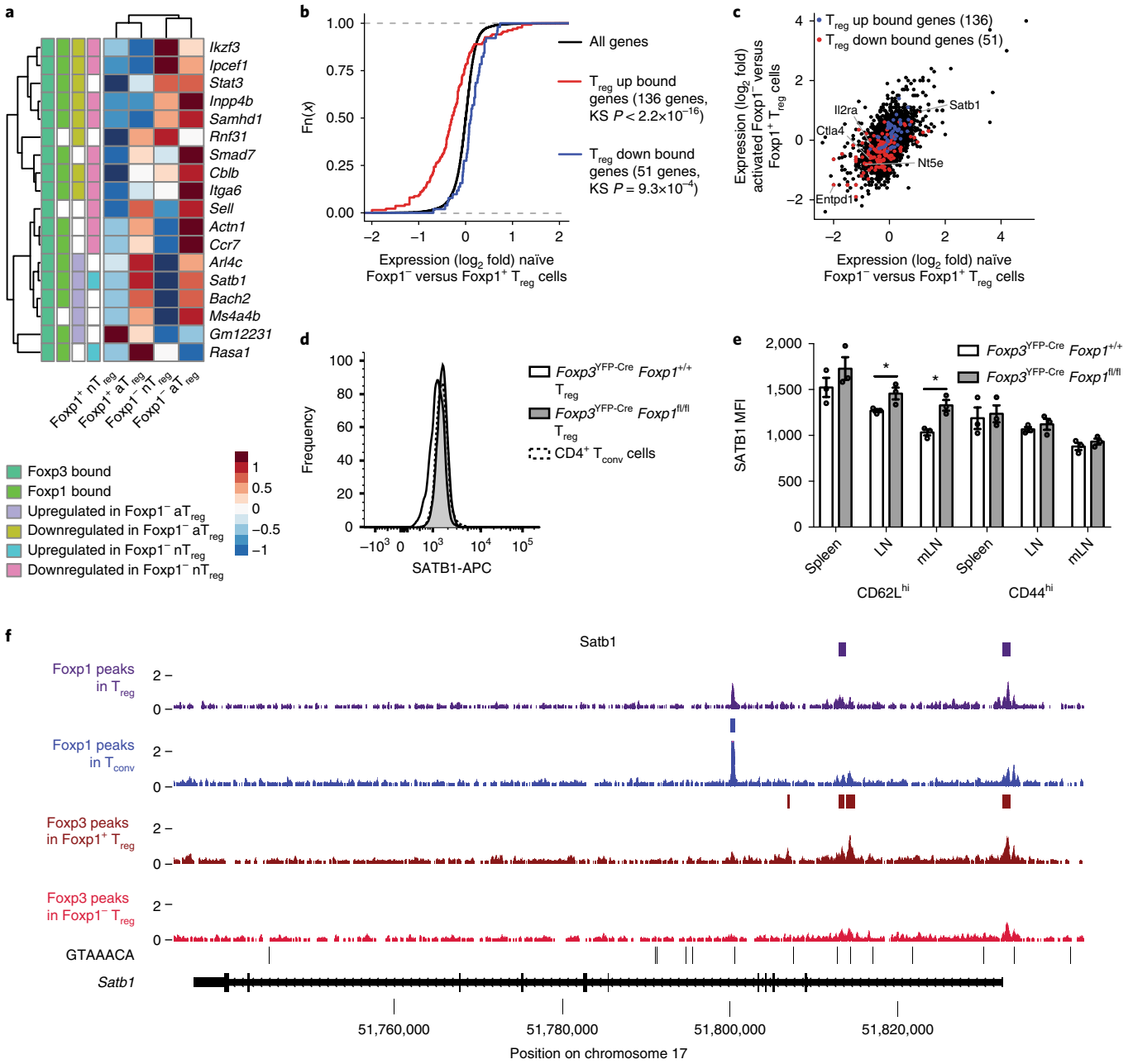

Fig. 3 | Foxp1-dependent regulation of gene expression in T_{reg} cells. a, Heat map comparing gene expression between Foxp1$^+$ and Foxp1$^-$ naïve and activated T_{reg} cells from *Foxp3*$^{YFP\text{-}Cre/+}$ *Foxp1*$^{+/+}$ or *Foxp1*$^{fl/fl}$ heterozygous female mice for a subset of genes associated with Foxp3 ChIP peaks with significantly higher Foxp3 ChIP-seq signal in *Foxp1*$^{+/+}$. **b**, Cumulative distribution plot showing expression of T_{reg} signature genes associated with Foxp3 or Foxp1 peaks in naïve Foxp1$^-$/Foxp1$^+$ T_{reg} cells. *P* values calculated using two-sided Kolmogorov–Smirnov (KS) test comparing T_{reg} signature genes to all genes. **c**, Fold change–fold change plot showing expression of T_{reg} signature genes associated with Foxp3 or Foxp1 peaks in naïve and activated Foxp1$^-$/Foxp1$^+$ T_{reg} cells. **d**, Representative histogram of SATB1 protein level in naïve Foxp1$^+$ and Foxp1$^-$ T_{reg} cells and in naïve T_{conv} cells (representative of two independent experiments). **e**, Summary plot of SATB1 MFI in Foxp1$^+$ and Foxp1$^-$ T_{reg} cells from 8- to 10-week-old male mice ($n = 3$ biologically independent mice per group, representative of two independent experiments, error bars represent s.e.m. centered on the mean, $^*P = 0.048$ (left) and $^*P = 0.012$ (right), unpaired two-tailed Student's *t*-test). **f**, Foxp3 and Foxp1 ChIP-seq tracks at the *Satb1* locus. Three biological replicates for ChIP-seq were used per genotype, except Foxp1$^+$ Treg cells, for which two replicates were used.

that expression of several functionally important T_{reg} cell signature genes, including *Ctla4*, *Il2ra*, *Nt5e* and *Entpd1*, was markedly reduced in comparison with Foxp1-sufficient T_{reg} cells. At the protein level, Foxp1-deficient T_{reg} cells in *Foxp3*$^{YFP\text{-}Cre}$*Foxp1*$^{fl/fl}$ mice expressed markedly lower amounts of CD25 and CTLA-4 (Fig. 4g). Notably, CD25 induction on T cell antigen receptor (TCR) stimulation was intact in Foxp1-deficient T_{conv} cells (Supplementary Fig. 5).

Thus, we investigated the suppressive function of Foxp1-deficient T_{reg} cells. Indeed, CD4$^+$ and CD8$^+$ T cells were more activated and more proliferative in mice harboring Foxp1-deficient T_{reg} cells than in control animals (Fig. 5a,b). We also observed increased production of IFN-γ and IL-2, but not IL-4 or IL-17, by CD4$^+$ T cells and IFN-γ by CD8 T cells (Fig. 5c,d; data not shown). Next, we adoptively co-transferred Foxp1-deficient or -sufficient T_{reg} cells with the T cells isolated from *Foxp3*^{DTR} mice harboring diphtheria

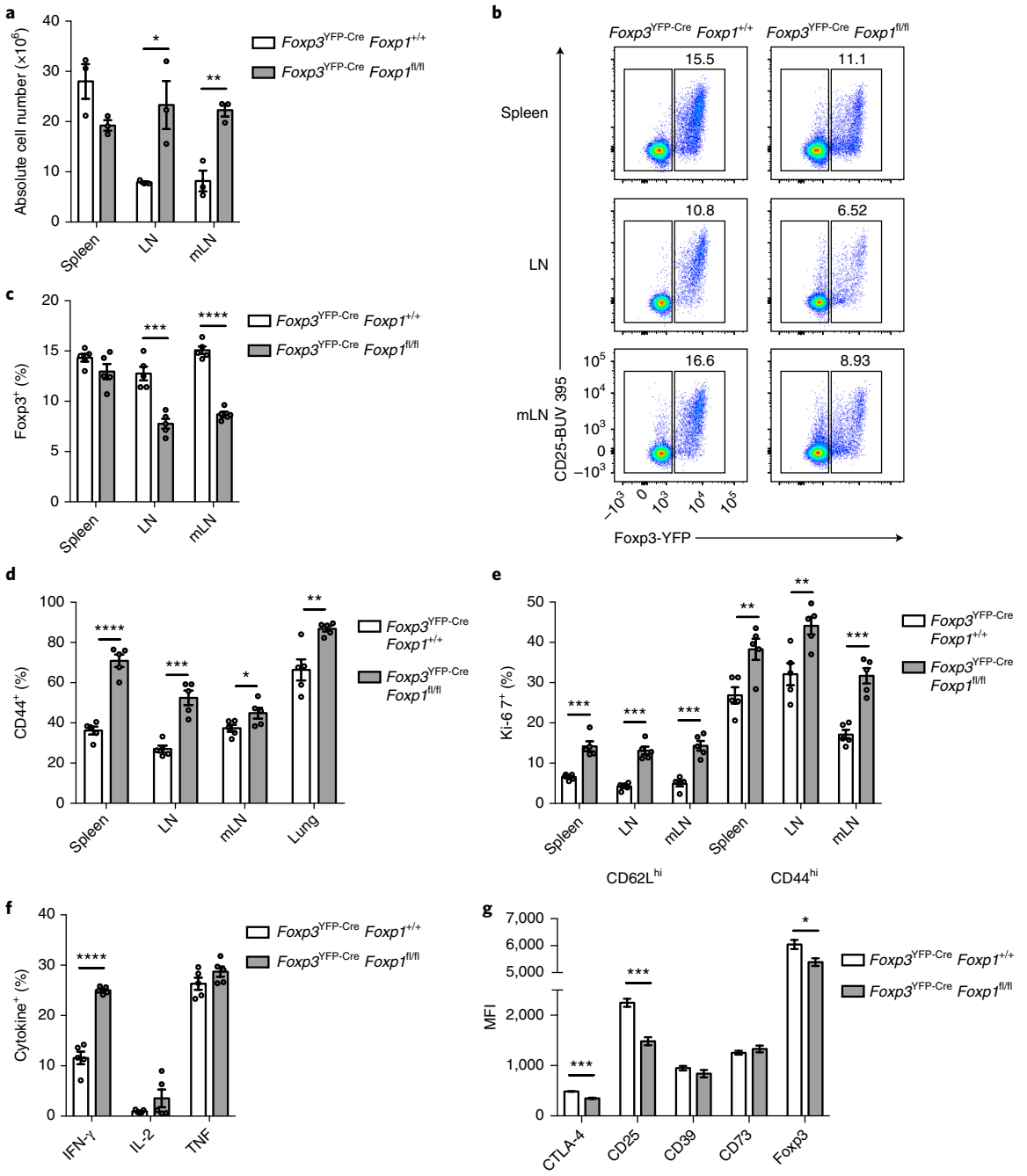

Fig. 4 | Foxp1 deficiency causes T_{reg} cell activation and effector cytokine production. a, Absolute cellularity of spleen, skin-draining lymph nodes (LN) and mesenteric lymph nodes (mLN) of 10-week-old male mice ($n = 3$ biologically independent mice per group, representative of several independent experiments, error bars represent s.e.m. centered on the mean, $^{*}P = 0.032$, $^{**}P = 0.0043$, unpaired two-tailed Student's t-test). **b**, Representative flow cytometric scatter plots gated on $CD4^+$ T cells from spleen, skin-draining lymph nodes and mesenteric lymph nodes of 10-week-old male mice showing Foxp3 and CD25 protein levels (representative of several independent experiments). **c**, Summary plot of $Foxp3^+$ T cell frequency among $CD4^+$ T cells in spleen, lymph nodes and mesenteric lymph nodes of 10-week-old mice ($n = 5$ biologically independent mice per group, representative of several independent experiments, error bars represent s.e.m. centered on the mean, $^{***}P = 0.0003$, $^{****}P = 0.0001$, unpaired two-tailed Student's t-test). **d**, $CD44^{hi}$ T_{reg} cell frequency among $Foxp3^+$ T_{reg} cells in various organs ($n = 5$ biologically independent mice per group, representative of several independent experiments, error bars represent s.e.m. centered on the mean, $^{****}P = 0.0001$, $^{***}P = 0.0002$, $^{*}P = 0.049$, $^{**}P = 0.0054$, unpaired two-tailed Student's t-test). **e**, Ki-67^+ T_{reg} cell frequency among all naïve $CD62L^{hi}$ or activated $CD44^{hi}$ T_{reg} cells ($n = 5$ biologically independent mice per group, representative of several independent experiments, error bars represent s.e.m. centered on the mean, $^{***}P = 0.0003$, $^{***}P = 0.0001$, $^{***}P = 0.0001$, $^{**}P = 0.0087$, $^{**}P = 0.009$, $^{***}P = 0.0002$ (left to right) unpaired two-tailed Student's t-test). **f**, Frequency of cytokine-producing T_{reg} cells among all splenic T_{reg} cells after 3 hours in vitro stimulation with PMA and ionomycin and with addition of brefeldin A ($n = 5$ biologically independent mice per group, representative of three independent experiments, error bars represent s.e.m. centered on the mean, $^{****}P < 0.0001$, unpaired two-tailed Student's t-test). **g**, Protein MFI of several T_{reg} signature proteins in splenic T_{reg} cells from male mice ($n = 5$ biologically independent mice per group, representative of several independent experiments, error bars represent s.e.m. centered on the mean, $^{***}P = 0.0001$, $^{***}P = 0.0002$, $^{*}P = 0.036$ (left to right), unpaired two-tailed Student's t-test).

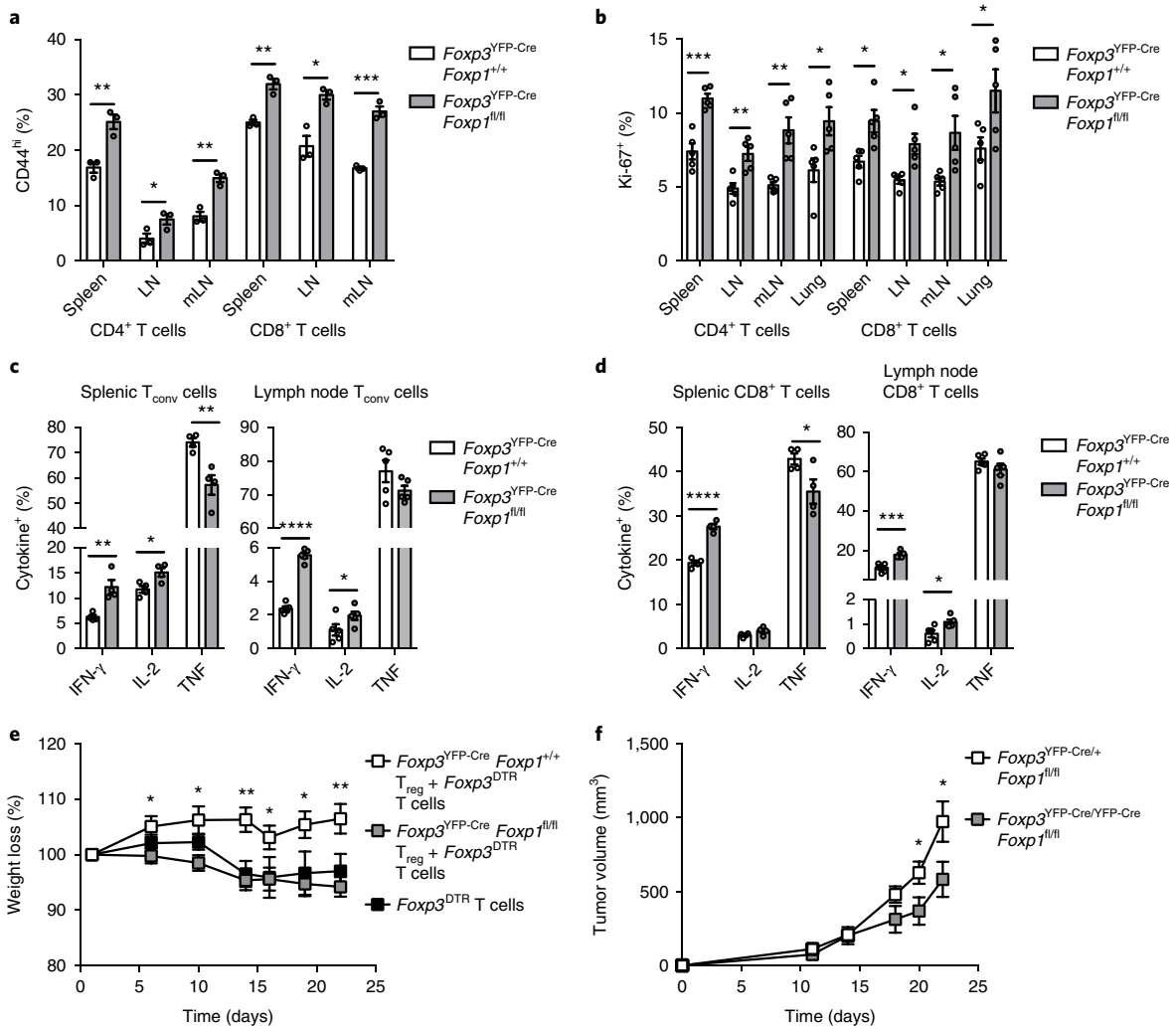

Fig. 5 | Foxp1 deficiency causes T_{reg} cell functional impairment. a, $CD44^{hi}$ cell frequency among splenic or lymph node $CD4^+$ T_{conv} cell or $CD8^+$ T cells ($n=3$ biologically independent mice per group, representative of several independent experiments, error bars represent s.e.m. centered on the mean, $^{**}P=0.0069$, $^{*}P=0.05$, $^{**}P=0.0033$, $^{**}P=0.0029$, $^{*}P=0.01$, $^{***}P=0.0004$ (left to right) unpaired two-tailed Student's *t*-test). **b**, $Ki\text{-}67^+$ T cell frequency among $CD4^+$ T_{conv} cells or $CD8^+$ T cells ($n=5$ biologically independent mice per group, representative of several independent experiments, error bars represent s.e.m. centered on the mean, $^{***}P=0.0005$, $^{**}P=0.004$, $^{**}P=0.003$, $^{*}P=0.028$, $^{*}P=0.012$, $^{*}P=0.01$, $^{*}P=0.02$, $^{*}P=0.04$ (left to right), unpaired two-tailed Student's *t*-test). **c**, Frequency of cytokine-producing T cells among all splenic and lymph node T_{conv} cells after 3 hours in vitro stimulation with PMA and ionomycin and with addition of brefeldin A ($n=5$ biologically independent mice per group, representative of three independent experiments, error bars represent s.e.m. centered on the mean, $^{**}P=0.00066$, $^{*}P=0.022$, $^{**}P=0.0072$, $^{****}P=0.0001$, $^{*}P=0.077$ (left to right), unpaired two-tailed Student's *t*-test). **d**, Frequency of cytokine-producing T cells among all splenic and lymph node $CD8^+$ T cells after 3 hours in vitro stimulation with PMA and ionomycin in the presence of brefeldin A ($n=5$ biologically independent mice per group, representative of three independent experiments, error bars represent s.e.m. centered on the mean, $^{****}P=0.0001$, $^{*}P=0.094$, $^{***}P=0.0009$, $^{*}P=0.024$ (left to right), unpaired two-tailed Student's *t*-test). **e**, Weight over time of T cell-deficient recipient mice adoptively transferred with $Foxp1^+$ or $Foxp1^-$ T_{reg} cells and $Foxp3^{DTR}$ T cells ($n=5$ biologically independent mice per group, representative of two independent experiments, error bars represent s.e.m. centered on the mean, $^{*}P=0.05$, $^{*}P=0.026$, $^{**}P=0.0046$, $^{*}P=0.036$, $^{*}P=0.011$, $^{**}P=0.0051$ (left to right), unpaired two-tailed Student's *t*-test). **f**, Tumor volume (mm^3) over time of E0771 breast cancer cell line in mammary fat pads of female mice ($n=4$ biologically independent mice per group with two tumors each, representative of two independent experiments, error bars represent s.e.m. centered on the mean, $^{*}P=0.049$, $^{*}P=0.049$ (left to right), unpaired two-tailed Student's *t*-test).

toxin receptor-expressing T_{reg} cells into T cell-deficient recipients and treated them with diphtheria toxin to deplete the $Foxp3^{DTR}$ T_{reg} cells. Mice that received Foxp1-deficient T_{reg} cells along with $Foxp3^{DTR}$ cells lost weight similarly to mice that received only $Foxp3^{DTR}$ T cells, while mice that received Foxp1-sufficient T_{reg} cells did not lose weight (Fig. 5e). The T_{conv} and $CD8^+$ T cells from the former produced more IFN-γ, IL-2 and TNF on stimulation by PMA plus ionomycin in comparison with those from control recipients expression (Supplementary Fig. 6). We found that fewer Foxp1-deficient T_{reg} cells remained at day 22 relative to Foxp1-sufficient T_{reg} cells, although they maintained Foxp3 (Supplementary Fig. 6). We also observed markedly delayed growth of a syngeneic breast carcinoma orthotopically transplanted into the mammary fat pads of female $Foxp3^{YFP\text{-}Cre}$ $Foxp1^{fl/fl}$ versus littermate control mice (Fig. 5f). Collectively, these results suggest that Foxp1 is required for T_{reg} cell suppressive function in vivo.

Cell-intrinsic effects of Foxp1 deficiency in T_{reg} cells. To distinguish between cell-intrinsic and -extrinsic effects of Foxp1 deficiency in T_{reg} cells, we analyzed $Foxp3^{YFP\text{-}Cre/+}$ $Foxp1^{fl/fl}$ heterozygous

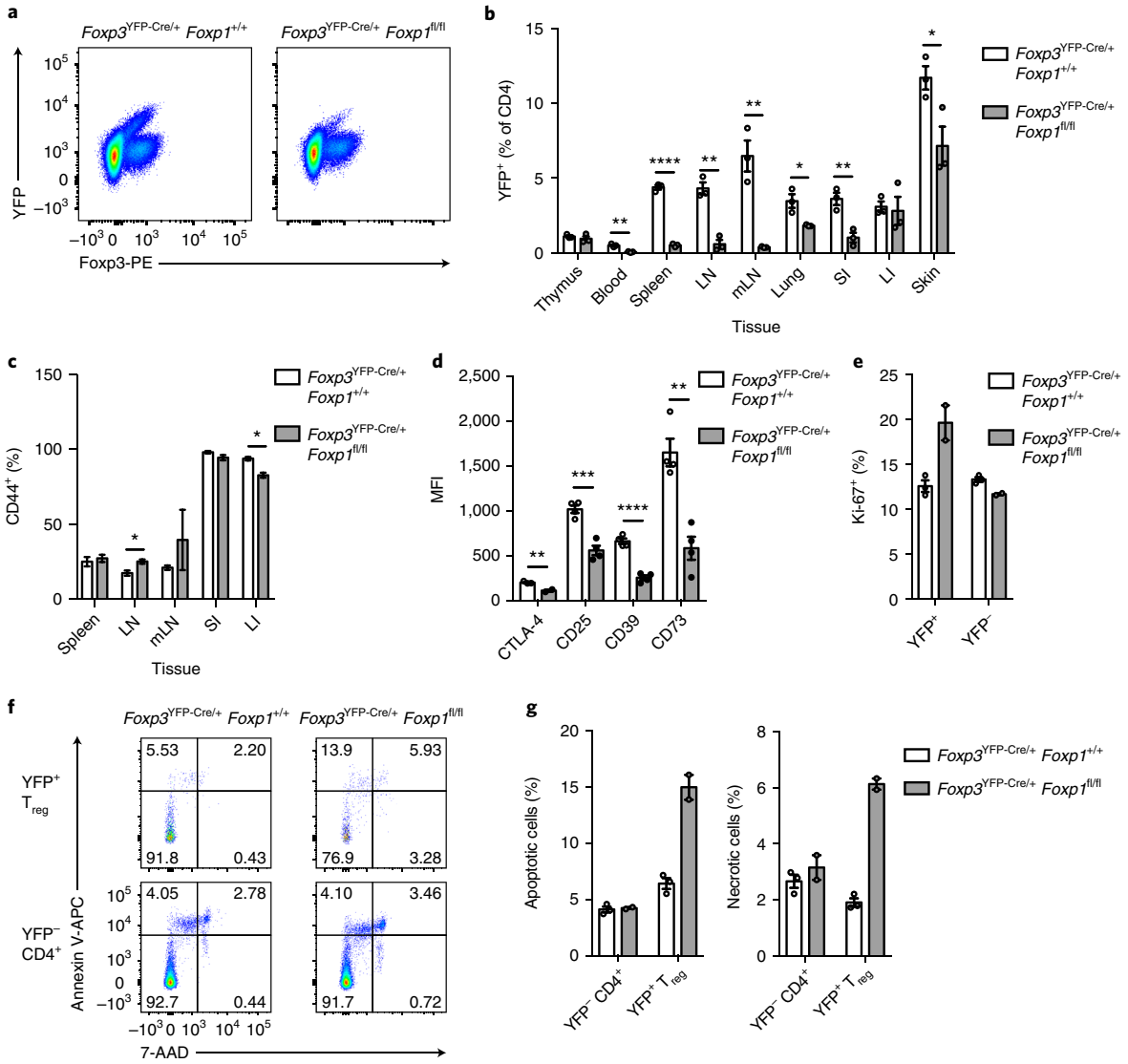

Fig. 6 | Cell-intrinsic effects of Foxp1 deficiency in T_{reg} cells. a, Representative flow cytometric scatter plots gated on CD4$^+$ T cells from spleens of 10-week-old *Foxp3*$^{YFP\text{-}Cre/+}$ *Foxp1*$^{+/+}$ or *Foxp1*$^{fl/fl}$ heterozygous female mice showing Foxp3 and YFP staining (representative of two independent experiments). **b**, YFP$^+$ T_{reg} cell frequency of CD4$^+$ T cells in 10-week-old heterozygous female mice in lymphoid and peripheral tissues ($n=3$ biologically independent mice per group, representative of three independent experiments, error bars represent s.e.m. centered on the mean, $^{**}P=0.003$, $^{****}P=0.0001$, $^{**}P=0.0016$, $^{**}P=0.0043$, $^{*}P=0.023$, $^{**}P=0.008$, $^{*}P=0.039$ (left to right), unpaired two-tailed Student's *t*-test). SI, small intestine; LI, large intestine. **c**, CD44^{hi} cell frequency among YFP$^+$ T_{reg} cells in lymphoid tissues of 10-week-old heterozygous female mice ($n=3$ biologically independent mice per group, representative of several independent experiments, error bars represent s.e.m. centered on the mean, $^{*}P=0.045$, $^{*}P=0.038$ (left to right), unpaired two-tailed Student's *t*-test). **d**, Protein MFI of several T_{reg} signature proteins in splenic YFP$^+$ T_{reg} cells from heterozygous female mice ($n=4$ biologically independent mice per group, representative of two independent experiments, error bars represent s.e.m. centered on the mean, $^{**}P=0.0086$, $^{***}P=0.0005$, $^{****}P=0.0001$, $^{**}P=0.0018$ (left to right), unpaired two-tailed Student's *t*-test). **e**, Ki-67$^+$ cell frequency among YFP$^+$ and YFP$^-$ T_{reg} cells in heterozygous female mice ($n=3$ biologically independent mice in control group and $n=2$ in experimental group, representative of two independent experiments, error bars represent s.e.m. centered on the mean). **f**, Representative flow cytometric scatter plots gated on YFP$^+$ T_{reg} cells or YFP$^-$ CD4$^+$ T cells from spleens of 10-week-old heterozygous female mice showing 7-AAD and annexin V staining (representative of two independent experiments). **g**, Summary plot of annexin V$^+$ 7-AAD$^-$ apoptotic and annexin V$^+$ 7-AAD$^+$ necrotic YFP$^+$ T_{reg} cells and YFP$^-$ CD4$^+$ T cells ($n=3$ biologically independent mice in control group and $n=2$ in experimental group, representative of two independent experiments, error bars represent s.e.m. centered on the mean).

female mice. Due to random X-chromosome inactivation, approximately half of the T_{reg} cells in these mice were expected to express YFP. Indeed, when *Foxp3*$^{YFP\text{-}Cre/+}$ *Foxp1*$^{+/+}$ heterozygous female mice were examined, 40% of the T_{reg} cells were YFP$^+$, indicating that expression of the *Foxp3*$^{YFP\text{-}Cre}$ protein confers a slight disadvantage to T_{reg} cells in a competitive setting (Fig. 6a). When we analyzed *Foxp3*$^{YFP\text{-}Cre/+}$ *Foxp1*$^{fl/fl}$ mice, we found that Foxp1-deficient YFP$^+$Foxp3$^+$ thymocytes were not competitively disadvantaged relative to Foxp1-sufficient Foxp3$^+$YFP$^+$ thymocytes. However, when we analyzed T_{reg} cells in the periphery we observed that Foxp1-deficient cells were severely outcompeted by Foxp1-sufficient ones (Fig. 6a,b). To gain insight into the mechanism underlying the reduced numbers of Foxp1-deficient T_{reg} cells in a competitive setting we assessed activation, proliferation and apoptosis of YFP$^+$ Foxp1-deficient T_{reg} cells in these mosaic mice. Foxp1 deficiency was shown to lead to cell-intrinsic activation of CD4$^+$ T_{conv} cells and CD8$^+$ T cells[12]. In contrast, Foxp1-deficient and -sufficient T_{reg} cells in heterozygous mice were activated to the same extent (Fig. 6c; data

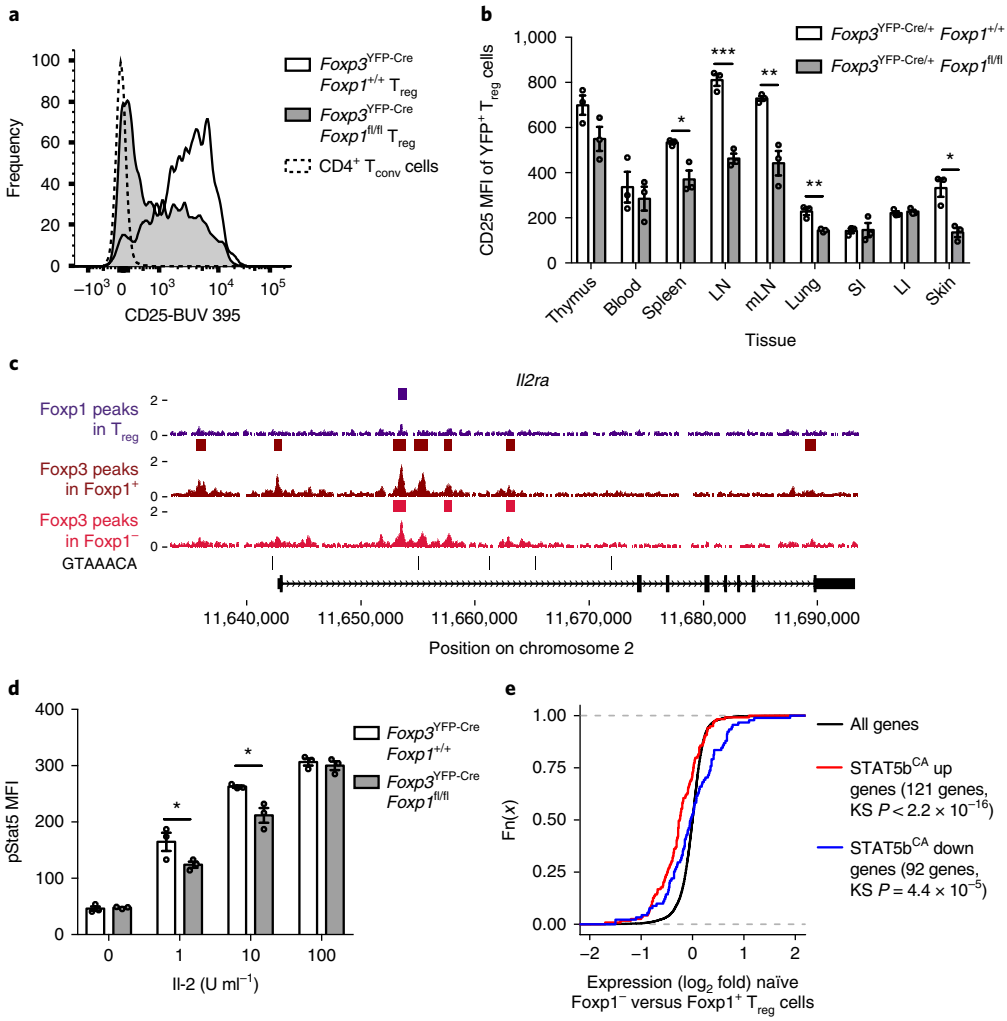

Fig. 7 | IL-2 signaling is impaired in Foxp1-deficient T_{reg} cells in a cell-intrinsic manner. a, Representative histograms of CD25 protein level in naïve Foxp1$^+$ and Foxp1$^-$ T_{reg} cells and in naïve T_{conv} cells (representative of several independent experiments). **b**, Summary plot of CD25 MFI in YFP$^+$ T_{reg} cells from heterozygous females ($n=3$ biologically independent mice per group, representative of three independent experiments, error bars represent s.e.m. centered on the mean, $^*P=0.094$, $^{***}P=0.015$, $^{**}P=0.0005$, $^{**}P=0.0065$, $^*P=0.011$ (left to right), unpaired two-tailed Student's *t*-test). SI, small intestine; LI, large intestine. **c**, Foxp3 and Foxp1 ChIP-seq tracks at the *Il2ra* locus (tracks show mean of three independent biological samples, Foxp1$^+$ T_{reg} track shows mean of two independent biological samples). **d**, IL-2 responsiveness of Foxp1$^+$ or Foxp1$^-$ sorted T_{reg} cells assessed by pSTAT5 MFI ($n=3$ biologically independent mice per group, representative of three independent experiments, error bars represent s.e.m. centered on the mean, $^*P=0.05$, $^*P=0.019$ (left to right), unpaired two-tailed Student's *t*-test). **e**, Cumulative distribution plot showing expression of STAT5B^{CA} signature genes in naïve Foxp1$^-$/Foxp1$^+$ T_{reg} cells. *P* values calculated using two-sided Kolmogorov–Smirnov (KS) test comparing STAT5B^{CA} signature genes with all genes.

not shown). Next we assessed expression of key molecules implicated in T_{reg} suppressor function in *Foxp3*$^{YFP\text{-}Cre/+}$ *Foxp1*$^{fl/fl}$ females. We observed diminished expression of CTLA-4 and CD25 in these mice (Fig. 6d). However, contrary to comparable CD39 and CD73 expression by Foxp1-sufficient and Foxp1-deficient T_{reg} cells in male *Foxp3*$^{YFP\text{-}Cre}$ *Foxp1*$^{fl/fl}$ and littermate control mice, their expression was noticeably reduced in Foxp1-deficient T_{reg} cells in comparison with Foxp1-sufficient T_{reg} cells in these mosaic mice (Fig. 6d). These experiments suggest that the aforementioned activated T_{reg} phenotype observed in *Foxp3*$^{YFP\text{-}Cre}$ *Foxp1*$^{fl/fl}$ mice was cell extrinsic and driven by increased activation of CD4$^+$ and CD8$^+$ T cells in response to impaired T_{reg} suppression.

Despite being comparably activated, YFP$^+$ Foxp1-deficient T_{reg} cells in *Foxp3*$^{YFP\text{-}Cre/+}$ *Foxp1*$^{fl/fl}$ heterozygous females were more proliferative than Foxp1-sufficient T_{reg} cells (Fig. 6e). Next, we examined the rate of apoptosis of YFP$^+$ Foxp1-deficient and Foxp1-sufficient T_{reg} cells in *Foxp3*$^{YFP\text{-}Cre/+}$ *Foxp1*$^{fl/fl}$ heterozygous female mice using annexin V staining. The percentages of annexin V-positive but 7-amino-actinomycin D (7-AAD)-negative YFP$^+$ T_{reg} cells were increased in the absence of Foxp1, while frequencies of apoptotic cells within YFP$^-$ T_{reg} cell subsets were comparable (Fig. 6f,g; data not shown). Thus, Foxp1 deficiency in T_{reg} cells has both cell-intrinsic and -extrinsic effects.

IL-2 signaling is impaired in Foxp1-deficient T_{reg} cells. IL-2 signaling is critical for T_{reg} cell suppressive function and for competitive fitness of T_{reg} cells[31], both of which are impaired in the context of Foxp1 deficiency, suggesting that a major functional consequence of Foxp1 loss in T_{reg} cells is dysregulation of CD25 expression. The diminished competitive fitness of Foxp1-deficient T_{reg} cells was consistent with markedly diminished expression of CD25 in comparison with Foxp1-sufficient ones. The lower expression of CD25 was also observed in YFP$^+$ T_{reg} cells from *Foxp3*$^{YFP\text{-}Cre/+}$ *Foxp1*$^{fl/fl}$ female mice, indicating that it was cell intrinsic (Fig. 7a,b). We also observed that Foxp1 and Foxp3 shared a binding site within the *Il2ra* locus. Although Foxp3 remained significantly bound to this

site in the absence of Foxp1, Foxp3 binding at several other sites within the *Il2ra* locus was reduced or lost in Foxp1-deficient T_{reg} cells (Fig. 7c).

To assess whether lower CD25 expression by Foxp1-deficient T_{reg} cells resulted in lower IL-2 responsiveness, we stimulated T_{reg} cells with varying concentrations of IL-2 and assessed STAT5 phosphorylation (Fig. 7d). We found that at low doses of IL-2 STAT5 was significantly less phosphorylated in Foxp1-deficient T_{reg} cells but that this difference was absent at high doses (Fig. 7d). IL-2 receptor-dependent activation of the transcription factor STAT5 has an essential role in the suppressor function of T_{reg} cells[31]. The STAT5 and TCR signaling pathways control largely distinct sets of genes and aspects of T_{reg} cell suppressor activity[31,32]. We analyzed the expression of the STAT5 activation-dependent gene set in our RNA-seq datasets and found that genes upregulated on STAT5 activation were more highly expressed by Foxp1-sufficient T_{reg} cells, whereas genes downregulated in a STAT5 activation-dependent manner were more highly expressed by Foxp1-deficient ones (Fig. 7e and Supplementary Table 5)[31]. Together, these results demonstrated that IL-2 signaling was severely impaired in Foxp1-deficient T_{reg} cells. Next, we tested whether saturating amounts of IL-2 could also restore key T_{reg} cell features affected by Foxp1 deficiency and observed a full restoration of CD25 and a pronounced partial rescue of Foxp3 and CTLA-4 expression in Foxp1-deficient T_{reg} cells. In contrast, we did not observe a rescue of SATB1 expression pattern in these cells (Supplementary Fig. 7). Thus, Foxp1 has an essential non-redundant function in T_{reg} cells by enforcing Foxp3-mediated regulation of expression of several characteristic T_{reg} lineage genes that can be partially rescued by provision of potent IL-2 signaling.

Discussion

T_{reg} cells were first identified as a $CD25^+CD4^+$ T lymphocyte subset[33]. Expression of Foxp3 during T_{reg} cell differentiation is associated with acquisition of distinct phenotypic and functional features, including high levels of CD25 and CTLA-4, and suppressor capacity and fitness[2,3,34–36]. Foxp3 is a member of the Foxp subfamily of transcription factors, which emerged as the result of two sequential ancestral gene duplication events during the invertebrate-to-vertebrate transition with a common ancestor, potentially giving rise to Foxp1 and the other three Foxp proteins[37]. Foxp1 plays an essential role in heart, central nervous system and lung development, in tumor progression in multiple cancer types[23,26,38–43] and in immune cell differentiation[10–12,44].

In this study we demonstrated that the close relative of Foxp3, Foxp1, exerts a non-redundant function in T_{reg} cells. Our experiments show that persistent expression of Foxp3 in resting and activated T_{reg} cells is not sufficient to supplant the function of Foxp1. Foxp1 and Foxp3 ChIP-seq analyses of T_{reg} and T_{conv} cells revealed that Foxp1 was bound to a large subset of sites occupied by Foxp3. Foxp1 binding in T_{reg} and T_{conv} cells was highly overlapping and predominantly observed at promoter regions of target genes, and very few Foxp1-occupied sites were not bound by Foxp3 in T_{reg} cells. The remarkable co-occurrence of Foxp1 binding sites in both T_{conv} and T_{reg} cells with those occupied by Foxp3 binding was in contrast to a previously reported loss of Foxo1 from a subset of Foxo1-bound sites in T_{conv} cells and gain of Foxp3 binding to these sites in T_{reg} cells[17]. These results suggest that Foxp1 probably acts cooperatively and synergistically with Foxp3 in T_{reg} cells rather than acting like Foxo1 as a 'predecessor' of Foxp3. Consistently, several reports describe antagonistic roles of Foxo1 and Foxp1 at certain loci, including *Il7ra* and *Il9*[12,44].

Despite the fact that Foxp1 was bound only to a subset of Foxp3-bound sites, Foxp1 loss resulted in diminished genome-wide occupancy of Foxp3. Foxp1 therefore maintains Foxp3 occupancy at its target genes, probably by binding to a subset of its targets and enabling Foxp3 complexes lacking Foxp1 to bind elsewhere. Thus, it seems reasonable to assume that loss of Foxp1 in T_{reg} cells results in an overall diminution in Foxp(1 + 3) protein concentration resulting in Foxp3 complex 'redistribution' among the 'Foxp1/3 shared' and 'Foxp3-only' bound sites. This assumption is consistent with the observation that Foxp1 'assists' Foxp3 binding to DNA, potentially through heterodimerization, and the observation that sites occupied by Foxp1 in naïve T cells remain bound by both Foxp1 and Foxp3 in T_{reg} cells.

Although the DNA-binding domains of Foxp1 and Foxp3 are highly conserved, these proteins have pronounced sequence divergence at the N terminus; Foxp3 is also truncated at the C terminus in comparison with Foxp1[5]. Foxp3 is a component of large and heterogeneous 400–800 kDa multiprotein complexes, which include Foxp1, Runx1 and its essential cofactor CBFβ and other DNA-binding transcription factors[14,17]. CBFβ deficiency in T_{reg} cells had no effect on expression of CD25 or CTLA-4, but did lead to increased proportions of $GITR^{hi}$, $ICOS^{hi}$ and Ki-67^+ cells, indicative of T_{reg} cell activation[45]. In contrast to Runx1/CBFβ deficiency, Foxp1-deficient T_{reg} cells had dysregulated expression of certain Foxp3-bound genes that constitute the core T_{reg} cell signature, including CTLA-4 and CD25, and this dysregulation probably contributes to the observed impairment in T_{reg} cell functionality.

Unlike the cell-intrinsic loss of quiescence observed on Foxp1 ablation in $CD4^+$ and $CD8^+$ T cells, activation of Foxp1-deficient T_{reg} cells was not cell intrinsic. The activation state of Foxp1-sufficient and -deficient T_{reg} cells was comparable in mosaic heterozygote $Foxp3^{YFP\text{-}Cre/+}$ $Foxp1^{fl/fl}$ mice, as was IL7R expression. Since Foxp3-mediated repression of IL7R expression has been reported[46,47], it is probable that Foxp3 is capable of repressing *Il7ra* expression in the absence of Foxp1. The observed T_{reg} cell activation in the context of Foxp1 deficiency appeared to be in response to $CD4^+$ and $CD8^+$ T cell activation, which was probably caused by the impaired suppressor function of Foxp1-deficient T_{reg} cells.

Cell-intrinsic effects of Foxp1 deficiency in T_{reg} cells included increased apoptosis, decreased CD25, CTLA-4, CD73 and CD39 expression, and increased expression of the genome organizer SATB1. Previous studies have demonstrated an important role for CD25 and CTLA-4 expression and for SATB1 repression in functional competence of T_{reg} cells: ablation of conditional *Il2ra* and *Ctla4* alleles resulted in a loss of T_{reg} cell function[31,48]. Furthermore, ectopic SATB1 expression in T_{reg} cells resulted in a loss of suppressor function and increased pro-inflammatory cytokine production[30]. In agreement with these observations, Foxp1-deficient T_{reg} cells relieved from SATB1 repression produced pro-inflammatory cytokines on TCR activation, potentially contributing to the observed functional impairment. Thus, Foxp1-mediated regulation of gene expression in T_{reg} cells, including positive regulation of CD25 and IL-2 signaling, as well as of CTLA-4, CD39 and CD73, and negative regulation of SATB1 expression, probably contributes to its non-redundant role in T_{reg} cell functionality.

Online content

Any methods, additional references, Nature Research reporting summaries, source data, statements of data availability and associated accession codes are available at https://doi.org/10.1038/s41590-018-0291-z.

Received: 22 June 2018; Accepted: 25 November 2018;
Published online: 14 January 2019

References

1. Josefowicz, S. Z., Lu, L. & Rudensky, A. Y. Regulatory T cells: mechanisms of differentiation and function. *Annu. Rev. Immunol.* **30**, 531–564 (2012).
2. Fontenot, J. D., Gavin, M. A. & Rudensky, A. Y. Foxp3 programs the development and function of $CD4^+CD25^+$ regulatory T cells. *Nat. Immunol.* **4**, 330–336 (2003).

3. Hori, S., Nomura, T. & Sakaguchi, S. Control of regulatory T cell development by the transcription factor *Foxp3*. *Science* **299**, 1057–1061 (2003).
4. Fontenot, J. D. et al. Regulatory T cell lineage specification by the forkhead transcription factor foxp3. *Immunity* **22**, 329–341 (2005).
5. Lam, E. W., Brosens, J. J., Gomes, A. R. & Koo, C. Y. Forkhead box proteins: tuning forks for transcriptional harmony. *Nat. Rev. Cancer* **13**, 482–495 (2013).
6. Zheng, Y. et al. Genome-wide analysis of Foxp3 target genes in developing and mature regulatory T cells. *Nature* **445**, 936–940 (2007).
7. Marson, A. et al. Foxp3 occupancy and regulation of key target genes during T-cell stimulation. *Nature* **445**, 931–935 (2007).
8. Song, X. et al. Structural and biological features of FOXP3 dimerization relevant to regulatory T cell function. *Cell Rep.* **1**, 665–675 (2012).
9. Hu, H. et al. Foxp1 is an essential transcriptional regulator of B cell development. *Nat. Immunol.* **7**, 819–826 (2006).
10. Wang, H. et al. The transcription factor Foxp1 is a critical negative regulator of the differentiation of follicular helper T cells. *Nat. Immunol.* **15**, 667–675 (2014).
11. Feng, X. et al. Foxp1 is an essential transcriptional regulator for the generation of quiescent naïve T cells during thymocyte development. *Blood* **115**, 510–518 (2010).
12. Feng, X. et al. Transcription factor Foxp1 exerts essential cell-intrinsic regulation of the quiescence of naïve T cells. *Nat. Immunol.* **12**, 544–550 (2011).
13. Li, B. et al. FOXP3 is a homo-oligomer and a component of a supramolecular regulatory complex disabled in the human XLAAD/IPEX autoimmune disease. *Int. Immunol.* **19**, 825–835 (2007).
14. Rudra, D. et al. Transcription factor Foxp3 and its protein partners form a complex regulatory network. *Nat. Immunol.* **13**, 1010–1019 (2012).
15. Gerstein, M. B. et al. Architecture of the human regulatory network derived from ENCODE data. *Nature* **489**, 91–100 (2012).
16. Heinz, S. et al. Simple combinations of lineage-determining transcription factors prime cis-regulatory elements required for macrophage and B cell identities. *Mol. Cell* **38**, 576–589 (2010).
17. Samstein, R. M. et al. Foxp3 exploits a pre-existent enhancer landscape for regulatory T cell lineage specification. *Cell* **151**, 153–166 (2012).
18. Koh, K. P., Sundrud, M. S. & Rao, A. Domain requirements and sequence specificity of DNA binding for the forkhead transcription factor FOXP3. *PLoS ONE* **4**, e8109 (2009).
19. Chen, Y. et al. DNA binding by FOXP3 domain-swapped dimer suggests mechanisms of long-range chromosomal interactions. *Nucleic Acids Res.* **43**, 1268–1282 (2015).
20. Zheng, Y. et al. Role of conserved non-coding DNA elements in the Foxp3 gene in regulatory T-cell fate. *Nature* **463**, 808–812 (2010).
21. Ono, M. et al. Foxp3 controls regulatory T-cell function by interacting with AML1/Runx1. *Nature* **446**, 685–689 (2007).
22. van der Veeken, J. et al. Memory of inflammation in regulatory T cells. *Cell* **166**, 977–990 (2016).
23. Zhang, Y. et al. Foxp1 coordinates cardiomyocyte proliferation through both cell-autonomous and nonautonomous mechanisms. *Genes Dev.* **24**, 1746–1757 (2010).
24. Hisaoka, T., Nakamura, Y., Senba, E. & Morikawa, Y. The forkhead transcription factors, Foxp1 and Foxp2, identify different subpopulations of projection neurons in the mouse cerebral cortex. *Neuroscience* **166**, 551–563 (2010).
25. Cesario, J. M., Almaidhan, A. A. & Jeong, J. Expression of forkhead box transcription factor genes Foxp1 and Foxp2 during jaw development. *Gene Expr. Patterns* **20**, 111–119 (2016).
26. Banham, A. H. et al. The FOXP1 winged helix transcription factor is a novel candidate tumor suppressor gene on chromosome 3p1. *Cancer Res.* **61**, 8820–8829 (2001).
27. Gabut, M. et al. An alternative splicing switch regulates embryonic stem cell pluripotency and reprogramming. *Cell* **147**, 132–146 (2011).
28. Hill, J. A. et al. Foxp3 transcription-factor-dependent and -independent regulation of the regulatory T cell transcriptional signature. *Immunity* **27**, 786–800 (2007).
29. Kitagawa, Y. et al. Guidance of regulatory T cell development by Satb1-dependent super-enhancer establishment. *Nat. Immunol.* **18**, 173–183 (2017).
30. Beyer, M. et al. Repression of the genome organizer SATB1 in regulatory T cells is required for suppressive function and inhibition of effector differentiation. *Nat. Immunol.* **12**, 898–907 (2011).
31. Chinen, T. et al. An essential role for the IL-2 receptor in T_{reg} cell function. *Nat. Immunol.* **17**, 1322–1333 (2016).
32. Levine, A. G., Arvey, A., Jin, W. & Rudensky, A. Y. Continuous requirement for the TCR in regulatory T cell function. *Nat. Immunol.* **15**, 1070–1078 (2014).
33. Sakaguchi, S., Sakaguchi, N., Asano, M., Itoh, M. & Toda, M. Immunologic self-tolerance maintained by activated T cells expressing IL-2 receptor alpha-chains (CD25). Breakdown of a single mechanism of self-tolerance causes various autoimmune diseases. *J. Immunol.* **155**, 1151–1164 (1995).
34. Khattri, R., Cox, T., Yasayko, S. & Ramsdell, F. An essential role for Scurfin in $CD4^+CD25^+$ T regulatory cells. *Nat. Immunol.* **4**, 337–342 (2003).
35. Lin, W. et al. Regulatory T cell development in the absence of functional Foxp3. *Nat. Immunol.* **8**, 359–368 (2007).
36. Gavin, M. A. et al. Foxp3-dependent programme of regulatory T-cell differentiation. *Nature* **445**, 771–775 (2007).
37. Song, X., Tang, Y. & Wang, Y. Genesis of the vertebrate FoxP subfamily member genes occurred during two ancestral whole genome duplication events. *Gene* **588**, 156–162 (2016).
38. Shu, W. et al. Foxp2 and Foxp1 cooperatively regulate lung and esophagus development. *Development* **134**, 1991–2000 (2007).
39. Shu, W., Yang, H., Zhang, L., Lu, M. M. & Morrisey, E. E. Characterization of a new subfamily of winged-helix/forkhead (Fox) genes that are expressed in the lung and act as transcriptional repressors. *J. Biol. Chem.* **276**, 27488–27497 (2001).
40. Tamura, S., Morikawa, Y., Iwanishi, H., Hisaoka, T. & Senba, E. Foxp1 gene expression in projection neurons of the mouse striatum. *Neuroscience* **124**, 261–267 (2004).
41. Wang, B. et al. Foxp1 regulates cardiac outflow tract, endocardial cushion morphogenesis and myocyte proliferation and maturation. *Development* **131**, 4477–4487 (2004).
42. Banham, A. H. et al. Expression of the FOXP1 transcription factor Is strongly associated with inferior survival in patients with Diffuse Large B-Cell Lymphoma. *Clin. Cancer Res.* **11**, 1065–1072 (2005).
43. Zabarovsky, E. R., Lerman, M. I. & Minna, J. D. Tumor suppressor genes on chromosome 3p involved in the pathogenesis of lung and other cancers. *Oncogene* **21**, 6915–6935 (2002).
44. Bi, E. et al. Foxo1 and Foxp1 play opposing roles in regulating the differentiation and antitumor activity of TH9 cells programmed by IL-7. *Sci. Signal.* **10**, eaak974 (2017).
45. Rudra, D. et al. Runx-CBFbeta complexes control expression of the transcription factor Foxp3 in regulatory T cells. *Nat. Immunol.* **10**, 1170–1177 (2009).
46. Liu, W. et al. CD127 expression inversely correlates with FoxP3 and suppressive function of human $CD4^+$ T reg cells. *J. Exp. Med.* **203**, 1701–1711 (2006).
47. Feuerer, M. et al. Genomic definition of multiple ex vivo regulatory T cell subphenotypes. *Proc. Natl. Acad.Sci. USA* **107**, 5919–5924 (2010).
48. Wing, K. et al. CTLA-4 control over Foxp3+ regulatory T cell function. *Science* **322**, 271–276 (2008).

Acknowledgements

We thank the Memorial Sloan Kettering Cancer Center (MSKCC) integrated genomics operation for sequencing RNA-seq and ChIP-seq libraries and preprocessing data. We thank A.C. Scott and D. Tran for help with tissue lymphocyte isolation and experiment optimization and all members of the A.Y. Rudensky laboratory for helpful discussions and technical assistance. This study was supported by NIH grants R37 AI034206 (A.Y.R.), P30 CA008748 (A.Y.R.) and U01 HG007893 (A.Y.R. and C.S.L.), as well as the Hilton–Ludwig Cancer Prevention Initiative funded by the Conrad N. Hilton Foundation and Ludwig Cancer Research (A.Y.R.). A.Y.R. is an investigator with the Howard Hughes Medical Institute.

Author contributions

C.K. and A.Y.R. conceived of and designed the experiments. C.K., Y.P., C.S.L. and A.Y.R. interpreted the results. C.K. and A.Y.R. wrote the manuscript. C.K. performed the experiments. Y.R. generated *Foxp1*^{fl} mice. Y.P. and C.S.L. designed computational analyses. Y.P. performed computational analyses.

Competing interests

The authors declare no competing interests.

Additional information

Supplementary information is available for this paper at https://doi.org/10.1038/s41590-018-0291-z.

Reprints and permissions information is available at www.nature.com/reprints.

Correspondence and requests for materials should be addressed to C.S.L. or A.Y.R.

Methods

Mice. Mice were bred and housed in the pathogen-free animal facility at Memorial Sloan Kettering Cancer Center and were used in accordance with institutional guidelines. Mouse experiments were approved by the Institutional Animal Care and Use Committee of Memorial Sloan Kettering Cancer Center. Unless otherwise noted, 8- to 10-week-old male and female sex-matched mice were used for all experiments. The *Foxp1* conditional targeting construct was designed to use two site-specific recombinations in vivo: (1) Flp recombinase to delete the *neo*^{r} marker from the mouse germline, and (2) Cre recombinase to conditionally delete *Foxp1* exon 11 flanked by two *lox*P sites. *Foxp1*$^{fl/+}$ mice (C57BL/6/129 mixed background) were backcrossed with C57BL/6 mice for at least five generations. Genotypes of *Foxp1*$^{fl/+}$, *Foxp1*$^{fl/fl}$ mice were determined by PCR amplification. The wild-type allele was identified by the production of a 376-bp PCR product and mutated *Foxp1* allele was identified by the production of a 257-bp PCR product (Supplementary Table 6). *Foxp1*$^{fl/fl}$ mice were crossed with *Foxp3*$^{YFP\text{-}Cre}$ transgenic mice to generate *Foxp3*$^{YFP\text{-}Cre/+}$*Foxp1*$^{fl/+}$ female mice. These mice were bred to *Foxp3*$^{+}$*Foxp1*$^{\lambda}$ male mice. *Foxp3*$^{YFP\text{-}Cre/+}$*Foxp1*$^{fl/fl}$ and *Foxp3*$^{YFP\text{-}Cre/+}$*Foxp1*$^{+/+}$ female offspring and *Foxp3*$^{YFP\text{-}Cre}$*Foxp1*$^{fl/fl}$ and *Foxp3*$^{YFP\text{-}Cre}$*Foxp1*$^{+/+}$ male offspring were used in experiments. In mammary tumor experiments, *Foxp3*$^{YFP\text{-}Cre/YFP\text{-}Cre}$*Foxp1*$^{fl/fl}$ mice were used as experimental mice and *Foxp3*$^{YFP\text{-}Cre/+}$*Foxp1*$^{fl/fl}$ mice were used as control mice. *Foxp1*$^{fl/fl}$ mice were crossed with *Cd4*^{Cre} transgenic mice to generate *Cd4*^{Cre}*Foxp1*$^{fl/+}$ mice. These mice were crossed to generate *Cd4*^{Cre}*Foxp1*$^{fl/fl}$ experimental and *Cd4*^{Cre}*Foxp1*$^{+/+}$ control mice. *Tcrb*$^{-/-}$*Tcrd*$^{-/-}$ mice and C57BL/6 *Ly5.1* mice were purchased from Jackson Laboratories and bred in-house. No blinding was performed during the mouse experiments.

Tissue lymphocyte isolation. For lymphocyte isolation from lung, mice were perfused with PBS and tissues were digested with collagenase A (1 mg ml^{-1}) and DNase I (1 unit ml^{-1}) for 45 min at 37 °C. For isolation of lamina propria lymphocytes, small and large intestines were first incubated with 1 mM EDTA and 1 mM dithiothreitol in PBS for 15 min at 37 °C. Samples were washed and incubated with collagenase A and DNase I for 40 min at 37 °C. Digested cell suspensions were filtered and lymphocyte-containing fractions were isolated using differential Percoll centrifugation.

Flow cytometry. Single-cell suspensions of cells were prepared from thymi, spleens, pooled axillary, brachial and inguinal lymph nodes, mesenteric lymph nodes, lungs and large and small intestines. For exclusion of dead cells, samples were first stained with Ghost Dye (Tonbo) cell viability reagent for 10 min in PBS on ice. Cells were then stained for 30 min on ice in FACS buffer (PBS, 2% fetal bovine serum, 2 mM EDTA) with antibodies against cell surface proteins. For downstream in vitro assays, cells were sorted into fetal bovine serum. For intracellular staining, cells were washed and fixed with Fix/Perm buffer (BD Biosciences) for 20 min on ice or with Foxp3-staining buffer (eBioscience) for 45 min on ice, washed and stained with antibodies against intracellular proteins (Supplementary Table 7). Stained cells were either analyzed on an LSRII flow cytometer (BD) or sorted using a FACSAria II cytometer (BD). Flow cytometry data were analyzed with FlowJo software (TreeStar).

Ex vivo stimulation. To measure T cell production of cytokines, single-cell suspensions were prepared from spleens, lymph nodes and mesenteric lymph nodes and cells were plated at 1×10^{6} cells in complete RPMI in round-bottom 96-well plates and treated with PMA (50 ng ml^{-1}; Sigma) and ionomycin (1 nM; Calbiochem) for 3 h in the presence of GolgiPlug (brefeldin A) and GolgiStop (monensin; BD Biosciences).

Ex vivo IL-2 responsiveness. To measure T_{reg} cell responsiveness to IL-2, CD62L^{+} naïve T_{reg} cells were isolated from lymphoid organs and plated at 1×10^{5} cells in complete RPMI in round-bottom 96-well plates and treated with IL-2 for 15 min at 37 °C. Cells were prepared for flow cytometric analysis according to the BD Phosflow protocol for mouse splenocytes (BD Biosciences). Cells were stained with anti-STAT5(p-Y694) (BD Biosciences).

Ex vivo apoptosis. To measure T cell apoptosis, single-cell suspensions were prepared from spleens, lymph nodes and mesenteric lymph nodes and 1×10^{6} cells were stained with annexin V and 7-AAD in Annexin V Binding Buffer (BD Biosciences).

CellTrace labeling and cell culture. YFP^{+} T_{reg} cells or CD62L^{+}CD4^{+} cells were sorted from pooled spleens and lymph nodes of *Foxp3*$^{YFP\text{-}Cre}$*Foxp1*$^{+/+}$, *Foxp3*$^{YFP\text{-}Cre}$*Foxp1*$^{fl/fl}$ and *Cd4*^{Cre}*Foxp1*$^{fl/fl}$ mice, washed twice with PBS and incubated for 10 min at 37 °C at a density of 1×10^{7} cells per ml in PBS with 1 μM CellTrace Violet (Invitrogen), then washed with complete RPMI. CellTrace-labeled cells were cultured for 7 days with or without recombinant mouse IL-7 (3 ng ml^{-1}; R&D systems) in complete RPMI at 37 °C. CellTrace profiles, cell viability and maintenance of CD4 or Foxp3 expression were assessed on day 7 by flow cytometry.

IL-2 cell culture. Single-cell suspensions were prepared from spleens, and from pooled axillary, brachial and inguinal lymph nodes. Cells were cultured for 24 h with or without human IL-2 (500 U ml^{-1}; NIH) in complete RPMI at 37 °C. T_{reg} cell viability and expression of CD25, CTLA-4, Foxp3 and SATB1 were assessed by flow cytometry.

In vivo suppression assay. CD4^{+} T cells (4×10^{5}) isolated from *Foxp3*$^{GFP\text{-}DTR}$*Ly5.1* were transferred together with YFP^{+} T_{reg} cells (1×10^{5}) isolated from *Foxp3*$^{YFP\text{-}Cre}$ *Foxp1*$^{fl/fl}$ or *Foxp3*$^{YFP\text{-}Cre}$ *Foxp1*$^{+/+}$ mice into T cell-deficient recipients. Recipients were treated with dithiothreitol on day 0, day 1 and then every 4 days post-transfer for the duration of the experiment. Weight was monitored throughout the experiment. T_{reg} cell frequencies in lymphoid and non-lymphoid tissues were analyzed at the experimental endpoint.

RNA sequencing. CD44^{hi} or CD62L^{hi} YFP^{+} Foxp1^{+} or Foxp1^{-} T_{reg} cell populations were FACS sorted from *Foxp3*$^{YFP\text{-}Cre/+}$*Foxp1*$^{+/+}$ and *Foxp3*$^{YFP\text{-}Cre/+}$*Foxp1*$^{fl/fl}$ mice directly into TriZol LS (ThermoFisher) and volume was adjusted post-sort. Samples were stored at −80 °C before RNA extraction. Total RNA was extracted and assessed for nucleic acid quantity and quality on the Agilent BioAnalyzer. SMARTer amplification with 12–16 cycles of PCR was followed by Illumina TruSeq paired-end library preparation following manufacturer's protocols. Samples were sequenced on the Illumina HiSeq 2500 to an average depth of 30 million, 50-bp read pairs per sample.

Chromatin immunoprecipitation and sequencing. FACS-sorted cell populations (2×10^{6} cells for Foxp3 ChIP-seq; 6×10^{6} cells for Foxp1 ChIP-seq) were cross-linked in 1% paraformaldehyde in PBS for 10 min at 21 °C. The reaction was quenched by addition of 125 mM glycine. Cross-linked cells were lysed and digested nuclei were resuspended in nuclear lysis buffer containing 1% SDS. Cells were sonicated for three rounds of 10×30 s with a Bioruptor (Diagenode) on high setting. Following sonication, chromatin was diluted with nuclear lysis buffer to final SDS concentration of 0.1% and precleared for 1 h at 4 °C with rotation with protein A/G magnetic beads (Pierce). Precleared DNA (5%) was saved as input. Chromatin was incubated overnight at 4 °C with rotation with polyclonal antibodies against Foxp3 (Rudensky laboratory) or Foxp1 (EMD Millipore ABE68). Immunocomplexes were incubated with protein A/G magnetic beads for 1 h at 4 °C with rotation. Immunocomplexes were precipitated and washed. After washing, precipitated chromatin and input DNA was decross-linked overnight at 65 °C in the presence of proteinase K, and DNA fragments were isolated using Qiagen PCR-purification kit. Purified DNA was processed for sequencing on Illumina HiSeq 2500 to an average depth of 30 million, 50-bp read pairs per sample. The resulting ChIP-seq samples are summarized in Supplementary Table 1.

Bioinformatics analyses. *Genome.* Mouse genome assembly mm10.GRCm38 was used for read alignments. Gene annotations from Ensembl (Mus_musculus. GRCm38.83) were used for all analysis. Unless otherwise noted, all analysis was done using R v3.4.0.

RNA-seq. Reads were aligned to the mouse genome using HISAT2 v2.0.1-beta[49] with default parameters including splice sites obtained from gene annotations. Uniquely aligned reads were extracted using grep with parameters '-v 'NH:i:[2–9]" and SAMtools v1.2[50] with parameters 'view -h -F 4 -q 20 -b' and sorted and indexed using SAMtools.

For analysis of RNA-seq in naïve or activated Foxp1^{+} or Foxp1^{-} T_{reg} cell samples, reads aligned to genes were counted using Rsubread v1.22.3[51] in R v3.3.0. Read counting for RNA-seq in naïve and activated T_{conv} and T_{reg} cells was done using R version 3.4.0, Rsubread v1.26.0.

Differential gene expression between any pair of cell states was assessed using DESeq2 v1.16.1[52], using default FDR adjustment of *P* values for multiple hypothesis testing. A total of 1,091 genes were detected as significantly differentially expressed between naïve Foxp1^{+} and Foxp1^{-} T_{reg} cells, and 2,353 genes were detected as significantly differentially expressed between activated Foxp1^{+} and Foxp1^{-} T_{reg} cells (FDR-adjusted $P<0.01$), for a total of 2,881 differentially expressed genes in either comparison. For visualization in heat maps and for clustering, read counts in genes were log-transformed (using $\log_2(\text{count}+1)$), and *z*-scores of the transformed counts per row were used. The $\log_2$fold change values were used to generate the cumulative distribution plot in Fig. 7e using STAT5-up and STAT5-down gene signatures listed in Supplementary Table 3. Significantly upregulated (163) or downregulated genes (108) in STAT5b^{CA} T_{reg} cells relative to their expression in control T_{reg} cells were defined as expressed genes with a $\log_2$fold change in expression of at least 1, and a FDR-adjusted $P\leq0.05$ (GSE84553).

ChIP-seq. Transcription factor ChIP-seq datasets for Foxp3 and Foxp1 were generated for Foxp1^{+} and Foxp1^{-} T_{reg} cells and Foxp1^{+} naïve T_{conv} cells (described in 'Chromatin immunoprecipitation and sequencing' section).

Reads were aligned to the mouse genome using Bowtie2 v2.2.5[53] with parameters '–no-unal -X 500 –no-mixed –no-discordant'. Uniquely aligned reads were extracted using SAMtools v1.1 with parameters 'view -h -bS -F 4 -q 20' and sorted and indexed using SAMtools.

For peak calling, MACS2 v2.1.1.20160309[54] was used with parameters '-f BAM -B –SPMR -g mm -p 0.1 –keep-dup 'auto' –call-summits'. For Foxp1, pooled

Foxp1$^+$ T_{reg} cells and Foxp1$^+$ T_{conv} cells ChIP-seq samples were used, with Foxp1$^-$ T_{reg} cell samples as control, to obtain a list of 55,265 putative peaks on standard chromosomes (chr1–chr19, chrX, chrY, chrM), with multiple summits per peak. ChIP-seq fragment length was estimated by MACS2 as 198 bp (Supplementary Fig. 1a). To obtain peaks with significant coverage in T_{reg} cells, ChIP-seq reads from each Foxp1$^+$ T_{reg} cell sample and from pooled control samples were counted in putative peaks using Rsubread v1.26.0, and DESeq2 v1.16.1 was applied to these counts, with FDR adjustment of *P* values for multiple hypothesis testing. To estimate sample size factors, DESeq2 was applied to read counts from the same samples in flanking regions of putative peaks, defined by shifting the putative peaks by 2 kilobases (kb) upstream and by 2 kb downstream and taking only those flanking regions that do not overlap with the original putative peaks. Values of $\log_2$fold change ChIP-seq for Foxp1 ChIP over control estimated using these sample size factors were used in plots in Figs. 1d,e, 2a and Supplementary Fig. 1b. This analysis resulted in 3,071 Foxp1 peaks in T_{reg} cells at MACS2 $q < 0.05$ and DESeq2 FDR < 0.01 that contained 4,619 summits. The same procedure was applied to each Foxp1$^+$ T_{conv} cell sample and pooled control samples and resulted in 1,088 Foxp1 peaks in T_{conv} cells. Out of 3,071 Foxp1 peaks identified in T_{reg} cells, 881 peaks were also detected among 1,088 Foxp1 peaks in T_{conv} cells. However, out of these 3,071 Foxp1 peaks in T_{reg} cells, 2,521 peaks were detected as Foxp1 peaks in T_{conv} cells at a relaxed threshold (MACS2 $q < 0.05$ and DESeq2 FDR < 0.1), while 550 were not. Out of 1,088 Foxp1 peaks in T_{conv} cells, 1,049 peaks were detected as Foxp1 peaks in T_{reg} cells at a relaxed threshold (MACS2 $q < 0.05$ and DESeq2 FDR < 0.1), while 39 were not.

The same procedure for peak calling was applied to pooled Foxp3 ChIP-seq samples from Foxp1$^+$ and Foxp1$^-$ T_{reg} cells, using Foxp3 ChIP-seq in Foxp1$^+$ and Foxp1$^-$ naïve T_{conv} cells as controls. This analysis resulted in 141,556 putative Foxp3 peaks on standard chromosomes, with estimated ChIP-seq fragment length also 198 bp (Supplementary Fig. 1a). The same procedure for significant ChIP-seq coverage assessment was applied to each Foxp3 ChIP-seq sample in Foxp1$^+$ T_{reg} cells and pooled control samples. The $\log_2$fold change ChIP-seq values of Foxp3 ChIP over control estimated using this procedure were used in plots in Figs. 1d,e, 2a and Supplementary Fig. 1b. This procedure resulted in 7,174 Foxp3 peaks in Foxp1$^+$ T_{reg} cells at MACS2 $q < 0.05$ and DESeq2 FDR < 0.01 that contained 13,997 summits. The same procedure applied to each Foxp3 ChIP-seq sample in Foxp1$^-$ T_{reg} cells and pooled control samples resulted in 3,935 Foxp3 peaks in Foxp1$^-$ T_{reg} cells.

Foxp3-only peaks were defined as those of 7,174 Foxp3 peaks in Foxp1$^+$ T_{reg} cells that did not overlap with any of the 55,265 putative Foxp1 peaks. This resulted in 1,101 Foxp3-only peaks that contained 1,956 summits. Foxp1-only peaks were defined as those of the 3,071 Foxp1 peaks in T_{reg} cells that did not overlap with any of 141,556 putative Foxp3 peaks. This resulted in 54 Foxp1-only peaks that contained 66 summits.

Each peak was associated with the closest gene according to distance in genomic coordinates, if this distance was not more than 20 kb. Peaks within 2 kb from a transcription start site of any annotated transcript were classified as promoter peaks; the remaining peaks were classified as exonic if overlapping with any exon of any annotated transcript; the remaining peaks were classified as intronic if within a gene body of any annotated gene; the remaining peaks within 20 kb of a gene were classified as intergenic; all the remaining peaks were left unclassified in this classification.

All Foxp3 and Foxp1 peaks detected with the above procedure are listed in Supplementary Table 2.

We performed *k*-means clustering of RNA-seq in Foxp1-bound genes that were differentially expressed between naïve Foxp1$^+$ and Foxp1$^-$ T_{reg} cells or between activated Foxp1$^+$ and Foxp1$^-$ T_{reg} cells (total of 661 genes), using function kmeans() in R. Gene ontology enrichment analysis was run using GOstats v2.44.0 and GO.db v3.5.0 in R.

For significant Foxp3 peaks in Foxp1$^+$ and Foxp1$^-$ T_{reg} cells, we applied DESeq2 to read counts from all Foxp1$^+$ and Foxp1$^-$ T_{reg} cell samples. Library size factors were estimated using read counts in flanking regions of the peaks, as described above, resulting in balanced estimates (Supplementary Fig. 1c, left). Then these library size factors were used for each sample in the read count analysis in actual peaks (Supplementary Fig. 1c, right). At FDR < 0.1, we identified 38 peaks (associated with 20 unique genes) with significantly stronger Foxp3 ChIP-seq signal in Foxp1$^-$ T_{reg} cell samples, and 94 peaks (associated with 53 unique genes) with significantly stronger Foxp3 ChIP-seq signal in Foxp1$^+$ T_{reg} cell samples. All significantly differentially expressed genes associated with any of these 94 peaks were used in the heat map in Fig. 3a. Cumulative distribution function plots of RNA-seq expression of genes associated with these differentially bound Foxp3 peaks between Foxp1$^+$ and Foxp1$^-$ T_{reg} cells are shown in Supplementary Fig 2b (first and third plots). The $\log_2$fold change Foxp3 ChIP-seq values of Foxp1$^-$ over Foxp1$^+$ estimated as described here were used in plots in Fig. 2b. As a control in Fig. 2b, $\log_2$fold change Foxp3 ChIP-seq values in the flanking regions of the peaks were used. As an additional control, $\log_2$fold change Foxp3 ChIP-seq values in accessibility peaks were used. For this, we pooled all ATAC-seq samples obtained from GEO (GSE83315)[22]. We aligned them to the genome and called the peaks in the same manner as described above for ChIP-seq. This resulted in 101,224 accessibility peaks at MACS2 $q < 0.01$. A total of 98.9% of our significant Foxp3 peaks (in either Foxp1$^+$ or Foxp1$^-$ T_{reg} cells) overlapped with these ATAC-seq peaks.

Sequence motifs in 150 bp windows around peak summits were identified de novo with HOMER[50], using script findMotifsGenome.pl with parameters 'mm10 -p 1 -size given -len 6,8,10,12 -noknown -mset vertebrates'. For Foxp3, 20 motifs were identified as significantly enriched, and 17 motifs were identified as significantly enriched for Foxp1. The top 10 most significant motifs were shown in Supplementary Fig 1. Then, for the identified motifs, their positions in the peak summits were identified using FIMO[55] with parameters '–no-qvalue –verbosity 1 –max-strand –thresh 0.01'. All motif occurrences of the most significant motifs (according to HOMER) with FIMO $P < 2 \times 10^{-4}$ are shown in Fig. 1. Runx family motifs were not detected as significantly enriched for Foxp1. We identified all individual occurrences of the forkhead motif in the Foxp3 peaks, and compared the number of peaks with more than two occurrences against a randomized number. For each randomization, we placed the same number of motif hits into the same number of peaks, placing each motif hit uniformly at random across peaks. We repeated this 10,000 times and calculated the expected number of peaks with two or more occurrences of the motif. The actual observed number of peaks with two or more occurrences of the forkhead motif was not larger than would be expected by chance.

Statistical analysis. All statistical analyses (excluding RNA-seq and ChIP-seq analyses) were performed using Prism7 (GraphPad Software). Differences between individual groups were analyzed for statistical significance using unpaired two-tailed Student's *t*-tests. *, $P \leq 0.05$; **, $P \leq 0.01$; ***, $P \leq 0.001$; ****, $P \leq 0.0001$. If no *, the difference is not significant ($P > 0.05$). Error bars show s.e.m. centered on the mean.

Reporting Summary. Further information on research design is available in the Nature Research Reporting Summary linked to this article.

Data availability

The datasets generated during the current study are included in this resource (and its supplementary information files) or are available in the Gene Expression Omnibus repository with accession code GSE121279. Datasets are relevant to Figs. 1, 2, 3, 7 and Supplementary Figs. 1, 3, 5. The ATAC-seq data relevant to Fig. 2 can be found in GEO (GSE83315) and the STAT5B^{CA} dataset relevant to Fig. 7 can be found in GEO (GSE84553). Detailed information on experimental design and reagents may be found in the Life Sciences Reporting Summary.

References

49. Kim, D., Langmead, B. & Salzberg, S. L. HISAT: a fast spliced aligner with low memory requirements. *Nat. Methods* **12**, 357–360 (2015).
50. Li, H. et al. The sequence alignment/map format and SAMtools. *Bioinformatics* **25**, 2078–2079 (2009).
51. Liao, Y., Smyth, G. K. & Shi, W. The Subread aligner: fast, accurate and scalable read mapping by seed-and-vote. *Nucleic Acids Res.* **41**, e108 (2013).
52. Love, M. I., Huber, W. & Anders, S. Moderated estimation of fold change and dispersion for RNA-seq data with DESeq2. *Genome Biol.* **15**, 550 (2014).
53. Langmead, B. & Salzberg, S. L. Fast gapped-read alignment with Bowtie 2. *Nat. Methods* **9**, 357–359 (2012).
54. Zhang, Y. et al. Model-based analysis of ChIP-Seq (MACS). *Genome Biol.* **9**, R137 (2008).
55. Grant, C. E., Bailey, T. L. & Noble, W. S. FIMO: scanning for occurrences of a given motif. *Bioinformatics* **27**, 1017–1018 (2011).

nature research

Corresponding author(s): Alexander Rudensky

Reporting Summary

Nature Research wishes to improve the reproducibility of the work that we publish. This form provides structure for consistency and transparency in reporting. For further information on Nature Research policies, see Authors & Referees and the Editorial Policy Checklist.

Statistical parameters

When statistical analyses are reported, confirm that the following items are present in the relevant location (e.g. figure legend, table legend, main text, or Methods section).

n/a	Confirmed	
☐	☒	The exact sample size (*n*) for each experimental group/condition, given as a discrete number and unit of measurement
☐	☒	An indication of whether measurements were taken from distinct samples or whether the same sample was measured repeatedly
☐	☒	The statistical test(s) used AND whether they are one- or two-sided *Only common tests should be described solely by name; describe more complex techniques in the Methods section.*
☐	☒	A description of all covariates tested
☐	☒	A description of any assumptions or corrections, such as tests of normality and adjustment for multiple comparisons
☐	☒	A full description of the statistics including central tendency (e.g. means) or other basic estimates (e.g. regression coefficient) AND variation (e.g. standard deviation) or associated estimates of uncertainty (e.g. confidence intervals)
☐	☒	For null hypothesis testing, the test statistic (e.g. *F*, *t*, *r*) with confidence intervals, effect sizes, degrees of freedom and *P* value noted *Give P values as exact values whenever suitable.*
☐	☒	For Bayesian analysis, information on the choice of priors and Markov chain Monte Carlo settings
☐	☒	For hierarchical and complex designs, identification of the appropriate level for tests and full reporting of outcomes
☐	☒	Estimates of effect sizes (e.g. Cohen's *d*, Pearson's *r*), indicating how they were calculated
☐	☒	Clearly defined error bars *State explicitly what error bars represent (e.g. SD, SE, CI)*

Our web collection on statistics for biologists may be useful.

Software and code

Policy information about availability of computer code

Data collection	Microsoft Excel v 14.7.1
Data analysis	R v3.3.0 GraphPad Prism v 7.0a

For manuscripts utilizing custom algorithms or software that are central to the research but not yet described in published literature, software must be made available to editors/reviewers upon request. We strongly encourage code deposition in a community repository (e.g. GitHub). See the Nature Research guidelines for submitting code & software for further information.

Data

Policy information about availability of data

All manuscripts must include a data availability statement. This statement should provide the following information, where applicable:

- Accession codes, unique identifiers, or web links for publicly available datasets
- A list of figures that have associated raw data
- A description of any restrictions on data availability

The datasets generated during and/or analyzed during the current study are included in this published article (and its supplementary information files) or are available in the Gene Expression Omnibus repository, GSE121279. Datasets are relevant to Fig. 1, 2, 3, 7 and Supplementary Fig. 3.

Field-specific reporting

Please select the best fit for your research. If you are not sure, read the appropriate sections before making your selection.

☒ Life sciences ☐ Behavioural & social sciences ☐ Ecological, evolutionary & environmental sciences

For a reference copy of the document with all sections, see nature.com/authors/policies/ReportingSummary-flat.pdf

Life sciences study design

All studies must disclose on these points even when the disclosure is negative.

Sample size	No formal power calculations were performed but n=3,4,5 were chosen because we anticipated that these sample sizes would be sufficient to identify differences between groups of laboratory mice.
Data exclusions	no data were excluded from the analyses.
Replication	All findings reported in this study were reproduced at least 3 times. ChIP-seq and RNA-seq data were not reproduced multiple times but were performed in biological triplicates.
Randomization	Samples were allocated into groups based on genotype. Samples were sex-matched and age-matched.
Blinding	Investigators were not blinded. Blinding was not relevant to the study because all analyses were strictly quantitative with no room for "subjective interpretation."

Reporting for specific materials, systems and methods

Materials & experimental systems

n/a	Involved in the study
☒	☐ Unique biological materials
☐	☒ Antibodies
☒	☐ Eukaryotic cell lines
☒	☐ Palaeontology
☐	☒ Animals and other organisms
☒	☐ Human research participants

Methods

n/a	Involved in the study
☐	☒ ChIP-seq
☐	☒ Flow cytometry
☒	☐ MRI-based neuroimaging

Antibodies

Antibodies used	See Supplementary Table 7.
Validation	Validation was performed with isotype controls in the lab prior to these experiments. Foxp1 antibody validation was performed using genetic controls (i.e. Foxp1-deficient cells stained with antibody). Satb1 antibody was validated by comparing staining of Treg cells (low Satb1) and CD4+ SP thymocytes (high Satb1) along with an isotype control antibody.

Animals and other organisms

Policy information about studies involving animals; ARRIVE guidelines recommended for reporting animal research

Laboratory animals	Described in detail in Methods.
Wild animals	The study did not involve wild animals.
Field-collected samples	The study did not involve samples collected from the field.

ChIP-seq

Data deposition

☒ Confirm that both raw and final processed data have been deposited in a public database such as GEO.

☒ Confirm that you have deposited or provided access to graph files (e.g. BED files) for the called peaks.

Data access links *May remain private before publication.*	GSE121279
Files in database submission	GSM3430729 Foxp1 ChIP-seq in Foxp1+ Treg, rep1 GSM3430730 Foxp1 ChIP-seq in Foxp1+ Treg, rep2 GSM3430731 Foxp1 ChIP-seq in Foxp1+ Treg, rep3 GSM3430732 Foxp1 ChIP-seq in Foxp1- Treg (genetic control) GSM3430733 Foxp1 ChIP-seq in conventional T cells, rep1 GSM3430734 Foxp1 ChIP-seq in conventional T cells, rep2 GSM3430735 Foxp3 ChIP-seq in Foxp1+ Treg, rep1 GSM3430736 Foxp3 ChIP-seq in Foxp1+ Treg, rep2 GSM3430737 Foxp3 ChIP-seq in Foxp1- Treg, rep1 GSM3430738 Foxp3 ChIP-seq in Foxp1- Treg, rep2 GSM3430739 Foxp3 ChIP-seq in Foxp1- Treg, rep3 GSM3430740 Foxp3 ChIP-seq in Foxp1+ conventional T cells, rep1 (genetic control) GSM3430741 Foxp3 ChIP-seq in Foxp1+ conventional T cells, rep2 (genetic control) GSM3430742 Foxp3 ChIP-seq in Foxp1+ conventional T cells, rep3 (genetic control) GSM3430743 Foxp3 ChIP-seq in Foxp1- conventional T cells, rep1 (genetic control) GSM3430744 Foxp3 ChIP-seq in Foxp1- conventional T cells, rep2 (genetic control) GSM3430745 Foxp3 ChIP-seq in Foxp1- conventional T cells, rep3 (genetic control)
Genome browser session (e.g. UCSC)	http://genome.ucsc.edu/cgi-bin/hgTracks?hgS_doOtherUser=submit&hgS_otherUserName=yuri.pritykin&hgS_otherUserSessionName=mm10%20Treg%20Foxp1%20Foxp3

Methodology

Replicates	YFP+ Treg or YFP- CD62Lhi CD4 T cells were pooled from 5 mice per replicate for Foxp1 ChIP-seq and pooled from 2 mice per replicate for Foxp3 ChIP-seq. For ChIP-seq in Treg cells, 3 Foxp1-sufficient and 3 Foxp1-deficient replicates were done. For naive Tconv ChIP-seq, 2 replicates were done.
Sequencing depth	30M paired end 50 bp reads.
Antibodies	Rabbit polyclonal Foxp3 antibody (Rudensky lab). Rabbit polyclonal Foxp1 antibody (Millipore ABE68).
Peak calling parameters	Described in detail in Methods.
Data quality	Described in detail in Methods.
Software	Described in detail in Methods.

Flow Cytometry

Plots

Confirm that:

☒ The axis labels state the marker and fluorochrome used (e.g. CD4-FITC).

☒ The axis scales are clearly visible. Include numbers along axes only for bottom left plot of group (a 'group' is an analysis of identical markers).

☒ All plots are contour plots with outliers or pseudocolor plots.

☒ A numerical value for number of cells or percentage (with statistics) is provided.

Methodology

Sample preparation	Described in detail in methods.
Instrument	Stained cells were either analyzed on a LSRII flow cytometer (BD) or sorted using a FACSAria II (BD).
Software	Flow cytometry data were analyzed with FlowJo software (TreeStar version 10.4.1).
Cell population abundance	Post-sort purity was verified by analyzing small aliquots of sorted samples on a FACSAria II (BD). Sample purity was always >95%.
Gating strategy	Samples were gated on FSC and SSC parameters to exclude debris and doublets. Samples were then gated to exclude dead cells and further gated to identify TCR-b+ CD4+, CD8+ and YFP+ cell populations.

☒ Tick this box to confirm that a figure exemplifying the gating strategy is provided in the Supplementary Information.